Integrin-deficient T cell leukemia accumulates in the central nervous system

Authors: Samantha Y. Lux[1,3], Cynthia Chen[1,3], Bibi S. Subhan[1], Martyna Okuniewska[1], Hyunsoo Chung[1], Jonah B. Vernejoul[1], Kathleen A. Martin[2], Asha Y. Caslin[2], Jennifer K. Schiavo[2], Robert C. Froemke[2], Michael Cammer[1], Susan R. Schwab[1,*]

Affiliations:
[1]Department of Cell Biology, New York University Grossman School of Medicine; New York, NY, USA.
[2]Neuroscience Institute, New York University Grossman School of Medicine; New York, NY, USA.

[3]These authors contributed equally.

[*]Corresponding author: Susan.Schwab@nyulangone.org

Summary

T cell acute lymphoblastic leukemia (T-ALL), a devastating childhood cancer, rapidly invades the central nervous system (CNS) and localizes to the meninges. T-ALL is aggressively treated with high-dose, CNS-directed chemotherapy; this regime results in lasting neurotoxicity and in some cases ultimately fails to protect from meningeal relapse. The paucity of knowledge about T-ALL entry and persistence in the CNS has limited the development of targeted therapies for decades. Here, we addressed whether VLA-4 and LFA-1, two integrins that mediate normal T cell entry to the CNS and that have been successfully targeted in patients for treatment of autoimmune disease, were similarly required in T-ALL. In the process, we uncovered an entirely unexpected role for these integrins in CNS disease. Not only were these integrins dispensable for T-ALL to reach the CNS, integrin-deficient T-ALL accumulated in the CNS compared to control T-ALL. Mechanistically, loss of integrins accelerated T-ALL proliferation in the CNS, suggesting that integrin-mediated interactions may promote quiescence in this space and highlighting the importance of niche-specific regulation of disease. Integrin blockade strongly synergized with anti-proliferative chemotherapy to treat CNS disease, indicating that combination therapy might be a powerful therapeutic strategy.

Introduction

Acute lymphoblastic leukemia (ALL) is the most common pediatric cancer.[1,2] In recent years, major advances have improved the five-year survival rate to over 90%.[2] However, ALL's propensity to infiltrate the central nervous system (CNS), particularly the meninges, remains a significant challenge.[3,4] To eradicate disease, the standard-of-care is to treat all children diagnosed with ALL with high-intensity, CNS-directed chemotherapy.[3,5] This regimen induces substantial toxicity and can cause irreparable neurological damage, substantially impacting patients' and their families' lives.[3,4] Furthermore, despite aggressive treatment, the CNS is a frequent site of relapse.[3,4] Our lack of understanding of how T-ALL enters and persists in the CNS has limited the development of targeted therapies for decades.

The T cell form of ALL, T-ALL, has especially high rates of CNS penetration.[6] Very little is known about how T-ALL infiltrates the CNS, but normal effector T cell trafficking into the CNS has been extensively characterized. T cells cross the blood endothelial barrier into the CNS through a stepwise process of rolling, sticking, and transmigration.[7] This cascade requires integrins—heterodimeric adhesion molecules consisting of an alpha and beta chain—which allow T cells to attach firmly to the endothelium.[7] The integrin VLA-4 ($\alpha 4\beta 1$) is canonically required for T cells to enter the CNS,[8,9] and in some cases the integrin LFA-1 can contribute to this transmigration.[7] In fact, natalizumab, a monoclonal antibody blocking the alpha subunit of VLA-4, is widely used to treat multiple sclerosis by preventing autoreactive T cells from reaching the brain.[10] Additionally, integrins enable B cell ALL to travel to the meninges via bridging channels between the skull bone marrow and the sub-arachnoid space.[11] We hypothesized that blocking VLA-4 and LFA-1 would render T-ALL unable to metastasize to the CNS.

Results

T-ALL deficient in LFA-1 and VLA-4 preferentially accumulates in the CNS

To test whether T-ALL could enter the CNS in the absence of LFA-1 and VLA-4, we developed a T-ALL cell line from mice that lacked these integrins (double-knockout, DKO), using an established protocol (Fig. S1A).[12] We chose a NOTCH1-driven model of T-ALL because mutations in *NOTCH1* and its regulators are found in the majority of human T-ALL cases.[13-15] In the integrin-deficient T-ALL cells, *Itgal* (αL, the alpha subunit of LFA-1) was knocked out,[16] and *Itgb1* (β1, the beta subunit of VLA-4) was excised.[17]

We co-transferred the DKO T-ALL cells at a 1:1 ratio with similarly generated, wild-type (WT) T-ALL cells intravenously into sub-lethally irradiated WT mice (Fig. 1A,B; Fig. S2A). At a humane endpoint, we enumerated DKO and WT T-ALL cells in common sites of disease (Fig. 1C,D). Surprisingly, in the CNS we found nearly 10 times more integrin-deficient T-ALL cells than WT T-ALL cells. This was especially remarkable considering the DKO T-ALL's relative absence in other tissues (Fig. 1C,D).

Of note, B cell ALL requires α6 integrin to enter the CNS, and β1 integrin is a canonical partner of α6. The DKO T-ALL cells lack $\alpha 6\beta 1$, and we could not detect α6 integrin or the other canonical binding partner of α6 integrin, β4 integrin, on the surface of these cells (Fig. S1B,C).[18,19]

Restoration of VLA-4 and LFA-1 in DKO T-ALL cells reduces CNS accumulation

To determine whether DKO T-ALL accumulation in the CNS was solely due to the absence of LFA-1 and VLA-4, we tested whether restoration of VLA-4 and LFA-1 in DKO T-ALL would reverse its accumulation in the CNS. We transduced the DKO T-ALL line with vectors encoding *Itgal* and *Itgb1* or an empty vector to generate "rescue" and "empty" lines (Fig. 1E). We found that restoration of αL and β1 in the DKO T-ALL (DKO-rescue) reduced the number of cells accumulating in the CNS compared to empty vector-transduced cells (DKO-empty) (Fig. 1F).

Deletion of VLA-4 and LFA-1 in WT T-ALL recapitulates CNS accumulation

To further test whether DKO T-ALL accumulation in the CNS was solely due to the absence of LFA-1 and VLA-4, we used CRISPR-Cas9 to target the first through third exons of *Itgal* and the first and second exons of *Itgb1* in the WT T-ALL line (Fig. 1G; Fig. S2B). These CRISPR-DKO T-ALL lines recapitulated the original phenotype, with CRISPR-DKO T-ALL preferentially accumulating in the CNS compared to control-targeted cells (CRISPR-WT) (Fig. 1H). We saw a similar phenotype when the DKO and WT T-ALL were transferred singly (Fig. 1I,J). Additionally, irradiation of the CNS was not required for DKO T-ALL to accumulate in the CNS (Fig. S3).

Taken together, these data suggest that loss of VLA-4 and LFA-1 integrins results in T-ALL accumulation within the CNS.

Integrin loss is unlikely to induce T-ALL accumulation in the CNS by enhancing CNS entry, limiting CNS exit, or promoting immune escape

Having disproven our original, seemingly obvious, hypothesis, we sought to explain how loss of integrins resulted in T-ALL accumulation in the CNS. It was possible that loss of integrins paradoxically improved entry into the CNS, limited exit from the CNS, or promoted T-ALL survival or proliferation within the CNS.

Entry: Up-regulation of other integrins

The most likely explanation for our results was that loss of VLA-4 and LFA-1 resulted in compensatory expression of other adhesion proteins that were better matched to adhesion molecules expressed by CNS blood endothelial cells in the context of leukemia. We performed bulk RNA sequencing comparing DKO and WT T-ALL isolated from the CNS and found few differentially expressed genes that might explain our phenotype (Fig. 2A, Fig. S4, Table S1). Among the integrins, only *Itgb7* was significantly increased in DKO compared to WT T-ALL. We confirmed elevated surface protein expression of β7 integrin (Fig. 2C), which might reflect a combination of increased mRNA and increased availability of its binding partner α4 integrin upon the loss of β1 integrin.

The ligand for α4β7 integrin, MAdCAM1, has primarily been characterized for its role in T cell migration into the gut,[20] but has also been found to be expressed in the choroid plexus during inflammation.[21] Furthermore, α4β7 integrin has been reported to facilitate T cell entry into the CNS in some settings.[22] To test whether DKO T-ALL was using α4β7 to cross into the CNS, we triply knocked out αL, β1, and β7 (third exon) in T-ALL cells using CRISPR-Cas9 as described above (Fig. 2C). We found that triple-knockout (TKO) T-ALL was indistinguishable from DKO T-ALL in its accumulation in the CNS (Fig. 2D). These results suggest that integrin α4β7 is not responsible for the increased accumulation of DKO T-ALL within the CNS.

Entry: Premature release from bone marrow

A second attractive explanation for our results was that loss of integrins led to premature release of T-ALL cells from the bone marrow, a key T-ALL niche. Integrins retain normal hematopoietic progenitor cells in the bone marrow; when VLA-4 binding is blocked, these cells exit their niche and move into the blood.[23-25] We hypothesized that this may be occurring in T-ALL, thus allowing DKO to migrate earlier to the CNS and take over the meningeal space. To test this, we conducted a time-course experiment, assessing the ratio of DKO:WT T-ALL in the CNS at different stages of disease. Contrary to our expectation, we found that WT T-ALL accumulated in the CNS before DKO T-ALL. At around mid-stage disease, DKO T-ALL caught up, and at late-stage disease, DKO T-ALL overtook WT leukemia (Fig. 2E, F).

Exit

We next hypothesized that DKO T-ALL may accumulate in the CNS due to a defective ability to exit the CNS. The dorsal lymphatics of the meningeal dura have been recently characterized as a key route of exit for lymphocytes from the CNS to the draining cervical lymph nodes,[26,27] and integrins in some cases enable T cells to access lymphatics.[28,29]

If DKO T-ALL accumulated in the CNS due to a failure to exit through the dorsal meningeal lymphatics, the ratio of DKO:WT T-ALL cells in the CNS should normalize in the absence of meningeal lymphatics. To ablate the meningeal lymphatics, we took advantage of the fact that, unlike most lymphatic vessels in the body, the dorsal meningeal lymphatics require continuous VEGFR3 signaling to persist.[30] We therefore treated mice with a "VEGF-trap," an adeno-associated virus encoding the ligand-binding domain of VEGFR3 fused to IgG-Fc, which captures available VEGFC/D and induces dorsal meningeal lymphatic regression. As a control, we treated mice with an adeno-associated virus that encodes the stalk (non-ligand-binding) of VEGFR3 fused to IgG-Fc.[30] Five weeks later, we induced leukemia in these animals by co-transferring WT and DKO T-ALL (Fig. 3A). We found that the regression of meningeal lymphatics had no effect on the ratio of the DKO to WT T-ALL in the CNS, or on the overall number of cells in the CNS (Fig. 3B). Meningeal lymphatic regression was confirmed by microscopy (Fig. S5A). We found similar results when we repeated this experiment using mice that were developmentally lacking in meningeal lymphatics (mice expressing the VEGF-trap under the keratin-14 promoter)[27] (Fig. S5B,C). These data suggest that DKO T-ALL does not preferentially accumulate in the CNS due to a requirement for integrins to exit through the meningeal lymphatics.

There may be alternate, uncharacterized pathways of exit from the CNS that could require integrins. To address more generally whether DKO T-ALL cells were defective in CNS egress compared to WT T-ALL cells, we labeled T-ALL cells in the CNS and assessed their location 48 hours later. Mice were surgically implanted with an intraventricular cannula in the lateral ventricle of the CNS prior to leukemia induction. Once mice reached mid-stage disease, we infused a reactive, fluorescent dye into the CNS via the cannula (Fig. 3C). 48 hours later, we found that T-ALL cells in the CNS were efficiently labeled. We found both labeled and non-labeled normal leukocytes in the CNS and the draining cervical lymph nodes, suggesting that normal leukocytes were cycling through the CNS. However, we did not detect labeled T-ALL cells in any other site, including blood, skull bone marrow, femoral bone marrow, spleen, or the CNS-draining cervical lymph nodes (Fig. 3D and not shown). Overall, we found no evidence that delayed exit causes accumulation of DKO T-ALL within the CNS.

Survival: Immune escape

As differences in trafficking seemed unlikely to explain the CNS accumulation of the DKO T-ALL, we next hypothesized that differential interactions with the host immune system might be responsible. Integrins play a key role in cementing synapses between leukocytes,[31] and cytotoxic T cells can have a powerful anti-tumor effect in ALL.[32,33] Perhaps the lack of integrins enabled the DKO T-ALL to escape immune surveillance.

If reduced susceptibility to an anti-leukemia immune response explained DKO T-ALL accumulation within the CNS, the ratio of DKO to WT T-ALL in the CNS should normalize in an immune-deficient host. To test this, we co-transferred WT and DKO T-ALL cells into NOD-*Rag1*$^{-/-}$*Il2rg*$^{-/-}$ (NRG) mice, which lack B, T, and NK cells, but found no difference in the ratio of the DKO:WT T-ALL in the CNS between the NRG mice and either WT C57BL/6 or NOD controls (Fig. 3E). Interestingly, the B6-derived leukemia was frequently cleared entirely in immune-competent NOD hosts (not shown). T-ALL cells also interact with myeloid cells, although integrin-mediated interactions with myeloid cells promote T-ALL progression in many tissues.[34,35] We tested a role of myeloid cells in the CNS accumulation of DKO cells by treating mice with the colony-stimulating factor 1 receptor (CSF1R) inhibitor PLX5622, which has been widely used to deplete microglia in the CNS[36] and been shown to deplete macrophages in peripheral tissues,[37,38] prior to induction of leukemia. We confirmed substantial depletion of CD45^{hi}CD11b^{+}Gr1^{-}CX3CR1^{+} cells in the spleen and CNS by flow cytometry (Fig. S6). We again found no difference in the ratio of DKO:WT T-ALL in the CNS between mice treated with the CSF1R inhibitor and controls (Fig. 3F). More generally, we did not observe a difference in the rate of apoptosis between DKO and WT T-ALL in the CNS, as assessed by flow cytometry of cells stained for cleaved caspase 3 (Fig. S7). Taken together, these data suggest that DKO T-ALL is not accumulating in the CNS because of its avoidance of an anti-leukemia immune response.

The loss of integrins in T-ALL confers a proliferation advantage in the CNS

DKO T-ALL proliferates more rapidly than WT T-ALL in the CNS

Within the meninges, we observed that the DKO and WT T-ALL localized differently—the DKO cells tended to spread through the tissue while the WT cells tended to cluster near blood vessels (Fig. 4A). This is consistent with observations of altered effector T cell motility within the spinal cord meninges upon intrathecal injection of integrin-blocking antibodies.[22,39] We hypothesized that this difference in distribution might result in differential access to nutrients, which are highly limiting in the CNS, or differential signals from the stromal niche, which might be unique in the CNS, and in turn affect proliferation.

We therefore performed an *in vivo* pulse-labelling experiment with 5-ethynyl-2′-deoxyuridine (EdU) and assessed the incorporation of EdU and the abundance of DNA by flow cytometry to identify proliferating cells (Fig. 4B). We observed a significant number of proliferating DKO and WT T-ALL cells in the CNS, bone marrow, and spleen, and found that DKO T-ALL was more proliferative than WT in both the bone marrow and CNS (Fig. 4C). Furthermore, the greatest difference between DKO and WT T-ALL proliferation was present in the CNS (Fig. 4D). When we repeated this experiment with the CRISPR-DKO and WT T-ALL pair, we again observed increased proliferation of DKO T-ALL in the CNS (Fig. 4E,F). Differences between the DKO and WT T-ALL in other tissues were less consistent between the two pairs of lines.

Interestingly, when comparing the proliferation rate of either DKO or WT T-ALL across tissues, there was little difference in the DKO T-ALL proliferation rate between spleen, bone marrow, and CNS; rather, the proliferation of the WT T-ALL was suppressed in the CNS when compared to spleen (Fig. 4C,E).

DKO T-ALL is more susceptible than WT T-ALL to 5-fluorouracil treatment

If increased proliferation of DKO compared to WT T-ALL cells in the CNS was in fact responsible for the increased accumulation of DKO compared to WT T-ALL in the CNS, the ratio of DKO:WT T-ALL should normalize if proliferation was limited. To test this, we treated mice at mid-stage disease with the thymidylate synthase inhibitor 5-flurouracil (5FU), a chemotherapy drug that targets dividing cells, for three days (Fig. 5A). We found that DKO T-ALL was depleted more than WT T-ALL in the CNS, where the ratio of DKO:WT T-ALL became nearly 1:1 in just three days (Fig. 5B). When we repeated this experiment with the CRISPR-DKO and WT T-ALL pair, we again observed a reduction in the ratio of DKO:WT T-ALL in the CNS with a short treatment (Fig. 5C). The efficacy of 5FU treatment was confirmed by enumerating total T-ALL in key tissues compared to vehicle-treated mice (Fig. S8).

DKO T-ALL has a proliferation advantage when co-cultured with meningeal fibroblasts

We hypothesized that the unique stroma of the CNS might be responsible for suppressing the proliferation of WT T-ALL. One of the most abundant cell types in the meninges is fibroblasts,[40-42] which have been shown to modulate the immune response in both infection and cancer.[41,43-47] To test this hypothesis, we co-cultured WT and DKO T-ALL cells with bulk fibroblasts isolated from the dural meninges of WT mice or with the OP9 stromal line, the T-ALL's normal feeder cells. After 3 days, we found that the ratio of DKO:WT cells significantly increased on the meningeal fibroblasts compared to the control OP9 line (Fig. 5D). We observed the same results when the assay was performed with the CRISPR-WT and CRISPR-DKO lines (Fig. 5E). To test whether the advantage of the DKO T-ALL reflected increased proliferation, we performed an EdU labelling assay in culture. We found that the proliferation of WT T-ALL was significantly less than DKO T-ALL after three days of co-culture with the meningeal fibroblasts (Fig. 5F). These data suggest that fibroblasts isolated from the meninges are sufficient to suppress the proliferation of WT T-ALL.

Integrin blockade synergizes with chemotherapy targeting proliferating cells to limit CNS T-ALL

One of the mainstays of therapy for ALL is to target rapidly proliferating cells with nucleotide-synthesis inhibitors.[3] We hypothesized that the efficacy of chemotherapy in the CNS could be improved by simultaneously blocking integrins: this strategy would force T-ALL cells to proliferate and thereby render them sensitive to the drugs. We used an intraventricular cannula to administer integrin-blocking antibodies to the CNS of mice with established WT T-ALL at the same time that they received systemic chemotherapy (5FU) (Fig. 6A). We confirmed the efficacy of blocking antibodies by flow cytometry (Fig. 6B). We found that the combination of intracranial blocking antibodies and systemic chemotherapy was far more effective at reducing total CNS T-ALL than chemotherapy alone (Fig. 6C). Mice that received intracranial antibodies without chemotherapy had no significant difference in CNS T-ALL accumulation from those that received isotype (fig. S9); however, they did experience a high rate of mortality (not shown).

Discussion

Much to our surprise, the loss of LFA-1 and VLA-4 in T-ALL did not block leukemia access to the CNS, but instead promoted T-ALL accumulation in the CNS. This finding was completely unexpected based on the precedent set by normal T cells and predictions from the T-ALL literature. It now seems improbable that T-ALL enters the CNS by crossing an intact endothelial barrier. Perhaps T-ALL either damages the endothelium to enter the CNS or migrates into the CNS via adjacent tissues, such as the bridging channels linking the skull bone marrow to the dura mater, although for B-ALL transit through the bridging channels has been shown to require integrins that T-ALL does not express.[11] An important future question for investigation is how T-ALL accesses the CNS without these canonical integrins: what route does it take into the meninges, and what are the mechanical requirements for this migration?

Mechanistically, integrin expression suppresses proliferation of T-ALL within the CNS. This finding introduces a second key question: how do integrins limit T-ALL proliferation in the CNS? The CNS is a canonically immune-suppressive environment, and the nature of CNS immune responses is an area of active research.[40,48-50] The discovery that exposure to meningeal fibroblasts can suppress proliferation of WT T-ALL in culture underscores the importance of understanding the stromal orchestration of CNS immune responses. While there are multiple types of meningeal fibroblasts with unique roles that are certainly not reflected in our assay,[40,41,50] our results suggest the hypothesis that T-ALL behavior reflects fundamental immune adaptations within the CNS. Stromal interactions with normal T cells may limit over-exuberant inflammatory responses and incidentally restrain T-ALL division.

Integrin blockade and anti-proliferative chemotherapy strongly synergize to treat CNS T-ALL. A series of important studies have interrogated the role of integrins in bone marrow ALL, primarily B-ALL. High integrin expression by ALL cells independently predicts poor prognosis,[35,51-54] and VLA-4 expression has been found to mediate chemoresistance of B-ALL in the bone marrow.[54-59] The finding that integrin blockade can render T-ALL more proliferative in the CNS reveals the need to understand what the fate of leukemia cells is when they are untethered from their niche. Thus, for example, integrin blockade alone was toxic in our model, but highly effective in combination with 5FU. Natalizumab, a blocking antibody against VLA4, is FDA-approved for treatment of multiple sclerosis, and additional drugs have been developed to target LFA1.[10,60] Ultimately, targeting integrins in T-ALL may be a powerful strategy to reduce the need for prolonged neurotoxic therapies.

Acknowledgments: We would like to thank members of the Schwab laboratory for helpful discussions throughout the duration of the project, and Eva Hernando and Shruti Naik for their insightful suggestions and review of the manuscript. We thank Kari Alitalo (University of Helsinki) for the VEGFR3 and control AAV and the K14-VEGFR3-Ig mice, and Iannis Aifantis (NYU School of Medicine) for the *Notch*Δ*E*-GFP/mCherry vectors. We are grateful to the NYU Langone Health Genome

Technology Center and Applied Bioinformatics Laboratories, especially Alireza Khodadadi-Jamayran, for assistance with RNA sequencing and bioinformatic analysis. We would like to thank the NYU Langone Health Division of Comparative Medicine animal technicians, especially Abdoul Fall, for their assistance.

Funding:

Blood Cancer Discoveries Grant from the Leukemia and Lymphoma Society, Mark Foundation for Cancer Research, and Paul G. Allen Frontiers Group (SRS)

NYU Center for Blood Cancers (SRS)

Vilcek Scholarship (SYL)

National Institutes of Health grant T32AI100853 (SYL, CC)

National Institutes of Health grant UL1RR029893 (CC)

National Institutes of Health grant F31AI154793 (MO)

National Institutes of Health grant R01HD088411 (RCF)

National Institutes of Health grant U19NS107616 (RCF)

National Institutes of Health/National Cancer Institute grant P30CA016087

Author contributions:

Conceptualization: SYL, CC, SRS

Methodology: MO, KAM, AYC, JKS, RCF, MC

Investigation: SYL, CC, HC, BSS, JBV

Formal analysis: SYL, CC

Visualization: SYL, CC

Funding acquisition: SRS

Project administration: SRS

Supervision: SRS

Writing – original draft: SYL, SRS

Writing – review & editing: SYL, CC, HC, BSS, SRS

Declaration of interests: SRS is an inventor on provisional patent 63/413,443 (Inhibitors of SPNS2 and uses thereof).

Data and materials availability: RNA sequencing expression data included in this study has been deposited in the NCBI Gene Expression Omnibus (GEO), accession number GSE244744

Supplementary Materials

Figs. S1 to S9

Table S1

Materials and Methods

Key resources table

REAGENT or RESOURCE	SOURCE	IDENTIFIER
Antibodies		
anti-B220 (clone RA3-6B2)	Biolegend	Cat#: 103201
anti-CD4 (clone GK1.1)	Biolegend	Cat#: 100401
anti-CD8 (clone 53-6.7)	Biolegend	Cat#: 100701
anti-CD11a (clone M17/4)	Biolegend	Cat#: 101101
anti-CD11b (clone M1/70)	Biolegend	Cat#: 101201
anti-CD25 (clone PC61)	Biolegend	Cat#: 102002
anti-CD31 (clone MEC13.3)	Biolegend	Cat#: 102501
anti-CD44 (clone IM7)	Biolegend	Cat#: 103001
anti-CD45 (clone 30-F11)	Biolegend	Cat#: 103101
anti CD45.1 (clone A20)	Biolegend	Cat#: 110702
anti-CD45.2 (clone 104)	Biolegend	Cat#: 109802
anti-CD49d (clone R1-2)	Biolegend	Cat#: 103603
anti-CD104 (clone 346-11A)	Biolegend	Cat#: 123602
anti-β7 (clone FIB504)	Biolegend	Cat#: 321202
anti-CX3CR1 (SA011F11)	Biolegend	Cat#: 149002
anti-GR1 (clone RB6-8C5)	Biolegend	Cat#: 108401
anti-Ter119 (clone TER-119)	Biolegend	Cat#: 116201
Streptavidin	Biolegend	Cat#: 405150
mouse IgG2a isotype control (clone MOPC-173)	Biolegend	Cat#: 400201
rat IgG2a, k isotype control (clone RTK2758)	Biolegend	Cat#: 400501
anti-CD4 (clone GK1.5)	eBioscience	Cat#: 14-0041-82
anti-CD29 (clone eBioHMb1-1)	eBioscience	Cat#: 11-0291-82
anti-Lyve1 (clone ALY7)	eBioscience	Cat#: 14-0443-82
Armenian Hamster IgG isotype control (clone eBio299Arm)	eBioscience	Cat#: 14-4888-81
anti-Active Caspase-3 (clone C92-605)	BD Bioscience	Cat#: 560627
CD16/32 (clone 93)	eBioscience	Cat#: 14-0161-82
anti-GFP	Abcam	Cat#: ab13970
anti-RFP	Rockland	Cat#: 600-401-379
Alexa Fluor 488 AffiniPure Goat Anti-Chicken IgY (IgG) (H+L)	Jackson ImmunoResearch	Cat#: 103-545-155
Alexa Fluor 647 AffiniPure Donkey Anti-Rabbit IgG (H+L)	Jackson ImmunoResearch	Cat#: 711-605-152
Cy3 Affinipure Donkey anti-Rabbit IgG (H+L) 1:1000 (Jackson ImmunoResearch)	Jackson ImmunoResearch	Cat#: 711-165-152
Anti-CD49d (clone PS/2)	BioXCell	Cat#: BE0071
anti-CD11a (clone M17/4)	BioXCell	Cat#: BE0006
Rat IgG2a, anti-trinitrophenol (clone 2A3)	BioXCell	Cat#: BE0089
Bacterial and virus strains		
AAV: AAV-VEGFR3(1-4)-Ig	Antila et al[30]	
AAV: AAV-VEGFR3(4-7)-Ig	Antila et al[30]	
Biological samples		

Chemicals, peptides, and recombinant proteins		
Flt3 ligand	PeproTech/ ThermoFisher	Cat#: 250-31
Stem Cell Factor	PeproTech/ ThermoFisher	Cat#: 250-03
Interleukin-3	PeproTech/ ThermoFisher	Cat#: 213-13
Interleukin-6	PeproTech/ ThermoFisher	Cat#: 216-16
Interleukin-7	PeproTech/ ThermoFisher	Cat#: 217-17
2-mercaptoethanol	Sigma Aldrich	Cat#: M3148
Ficoll-paque Premium	Cytiva	Cat#: 17544202
Percoll	Cytiva	Cat#: 17089101
Mitomycin C	Sigma Aldrich	Cat#: M5353
DAPI	Sigma Aldrich	Cat#: D9542
RNAse A	ThermoFisher	Cat#: EN0531
NHS-ester-Atto647	Sigma Aldrich	Cat#: 07376
PLX5622	MedChemExpress	Cat#: HY-114153
5-fluorouracil	Sigma Aldrich	Cat#: F6627
Collagenase D	MilliporeSigma	Cat#: 11088858001
DNAse I	Roche	Cat#: 04716728001
Dispase II	Roche	Cat#: 4942078001
Critical commercial assays		
Cytofix/Cytoperm	BD Bioscience	Cat#: BDB554714
LIVE/DEAD Fixable Far Red Dead Cell Stain Kit	ThermoFisher	Cat#: L34973
Click-iT Plus EdU Alexa Fluor 488/647 Flow Cytometry Assay Kit	ThermoFisher	Cat#: C10632/ C10634
RNeasy Plus Micro Kit	Qiagen	Cat#: 74034
RNAse-Free DNAse	Qiagen	Cat#: 79254
BioAnalyzer Pico	Agilent	Cat#: 5067-1513
DNA AMPure XP beads	Beckman-Coulter	Cat#: A63881
Nextera XT DNA library prep kit	Illumina	Cat#: FC-131-1024
Deposited data		
RNA sequencing expression data	This paper	GEO: GSE244744
Experimental models: Cell lines		
Mouse: Platinum-E retroviral packaging cells	Cell BioLabs Inc.	Cat#: RV-101
Mouse: OP9 cells	Nakano et al[61]	
Experimental models: Organisms/strains		
Mouse: C57BL/6 (CD45.2)	The Jackson Laboratory	Cat#: 000664
Mouse: B6.SJL-Ptprc^{a}Pepc^{b}/BoyJ (CD45.1)	The Jackson Laboratory	Cat#: 002014
Mouse: B6.Cg-Tg(Mx1-cre)1Cgn/J (Mx1-cre)[62]	The Jackson Laboratory	Cat#: 003556
Mouse: B6;129-*Itgb1*^{tm1Efu}/J (*Itgb1*f/f)[17]	The Jackson Laboratory	Cat#: 004605
Mouse: B6.129S7-*Itgal*^{tm1Bll}/J (*Itgal*$^{-/-}$)[16]	The Jackson Laboratory	Cat#: 005257
Mouse: NOD.Cg-*Rag1*^{tm1Mom} *Il2rg*^{tm1Wjl}/SzJ (NRG)[63]	The Jackson Laboratory	Cat#: 007799
Mouse: K14-VEGFR3-IG[64]	Mäkinen et al[64]	
Oligonucleotides		

sgRNA: *Itgb1*-1 Mm.Cas9.ITBG1.1.AB: 5' ACA UUC UCC GCA AGA UUG UUU UAG AGC UAG AAA UAG CAA GUU AAA AUA AGG CUA GUC CGU UAU CAA CUU GAA AAA GUG GCA CCG AGU CGG UGC 3'	IDT	
sgRNA: *Itgb1*-2 Mm.Cas9.ITBG1.1.AC: 5' GUC ACC AAU CGC AGC AAG UUU UAG AGC UAG AAA UAG CAA GUU AAA AUA AGG CUA GUC CGU UAU CAA CUU GAA AAA GUG GCA CCG AGU CGG UGC 3'	IDT	
sgRNA: *Itgal*-1 Mm.Cas9.ITGAL.1.AC: 5' GUA CUU GGG AAU GAC GCG UUU UAG AGC UAG AAA UAG CAA GUU AAA AUA AGG CUA GUC CGU UAU CAA CUU GAA AAA GUG GCA CCG AGU CGG UGC 3'	IDT	
sgRNA: *Itgal*-2 Mm.Cas9.ITGAL.1.AE: 5' GCC AAG AAG CUC UGC GUG UUU UAG AGC UAG AAA UAG CAA GUU AAA AUA AGG CUA GUC CGU UAU CAA CUU GAA AAA GUG GCA CCG AGU CGG UGC 3'	IDT	
sgRNA: *Itgb7*-1 Mm.Cas9.ITGB7.1.AA: 5' CAG CAC CGU UUU GUC CAC GAG UUU UAG AGC UAG AAA UAG CAA GUU AAA AUA AGG CUA GUC CGU UAU CAA CUU GAA AAA GUG GCA CCG AGU CGG UGC 3'	IDT	
sgRNA: *Itgb7*-2 Mm.Cas9.ITGB7.1.AC: 5' CGU GGA CCU AUA UUA CCU UAG UUU UAG AGC UAG AAA UAG CAA GUU AAA AUA AGG CUA GUC CGU UAU CAA CUU GAA AAA GUG GCA CCG AGU CGG UGC 3'	IDT	
Recombinant DNA		
Plasmid: MSCV-Notch1ΔE-IRES-GFP	Pitt et al[12]	
Plasmid: MSCV-Notch1ΔE-IRES-mCherry	Pitt et al[12]	
Plasmid: pMXs-IRES-mCherry	Cell BioLabs Inc.	Cat#: RTV-013
cDNA: Itgb1	Dharmacon/horizon	Cat#: 5721348
cDNA: Itgal	Dharmacon/horizon	Cat#: 40131105
Software and algorithms		
STAR aligner (v2.5.0c)	[65].	
Picard tools (v.1.126)	http://broadinstitute.github.io/picard	
HTSeq (v0.6.0)	[66]	
DEseq2[67]	[67]	
BEDTools (v2.17.0)	[68]	
bedGraphToBigWig tool (v4)	https://www.encodeproject.org/software/bedgraphtobigwig/	
R environment (v4.4)	(https://www.r-project.org/	

RStudio (v 2024.04.0+735)	https://posit.co/download/rstudio-desktop/	
R package: TidyVerse	https://www.tidyverse.org/	
DAVID	https://david.ncifcrf.gov/	
R package: ComplexHeatMap	Gu et al[69]	
R package: circlize	Gu et al[69]	
PRISM	GraphPad	
ImageJ	https://imagej.net/ij/index.html	
FIJI	https://imagej.net/software/fiji/	
FlowJo	https://www.flowjo.com/	
Zen	https://www.zeiss.com/microscopy/en/products/software/zeiss-zen.html	
LasX	https://www.leica-microsystems.com/products/microscope-software/p/leica-las-x-ls/	
FACSDiva	https://www.bdbiosciences.com/en-us/products/software/instrument-software/bd-facsdiva-software	
CytExpert	https://www.beckman.com/flow-cytometry/research-flow-cytometers/cytoflex/software	
Other		

Study design

The goal of this study was to understand the requirements for integrins in T-ALL infiltration of the central nervous system, and ultimately, to identify why integrin-deficient T-ALL accumulated in the CNS. Hypotheses were tested in mice *in vivo.* Sample sizes balanced statistical robustness and animal welfare. Group size reflects an effort to have multiple replicates of small groups (usually 2-4 distinct replicates with 3-5 mice in each group). The number of samples and the number of replicates for each experiment is indicated in figure legends. All findings were repeated multiple times in distinct experiments. No outliers were excluded, and no experiment was excluded unless a positive or negative control failed. These criteria were pre-established and are standard in the laboratory. Mice were randomly allocated to the experimental groups. The order of sample collection and data acquisition was designed to avoid experimental bias: collection and processing of samples from experimental and control groups was alternated. Investigators were not blinded, because there were no qualitative measurements.

Animals

C57BL/6 (CD45.2), B6.SJL-PtprcaPepcb/BoyJ (CD45.1), Mx1-cre[62], *Itgb1*$^{f/f}$[17], *Itgal*$^{-/-}$ [16] and NRG (NOD background, *Rag1*$^{-/-}$*Il2rg*$^{-/-}$[63]) mice were obtained from Jackson Laboratory. K14-VEGFR3-Ig mice were kindly provided by Kari Alitalo[64]. Mice were compared to littermate controls, unless otherwise specified. For CD45.2 or CD45.1/.2 hosts, female adult mice (6-12 weeks) were used. For all other hosts, male

and female adult mice (6-12 weeks) were used depending on availability, as sex did not seem to affect the results. Mice were housed in specific pathogen-free conditions at New York University School of Medicine animal facilities. All cages were on a 12-h light/dark cycle (light 06:00-18:00) in a temperature-controlled and humidity-controlled room. Room temperature was maintained at 72 ± 2 °F (22.2 ± 1.1 °C), and room humidity was maintained at 30–70%. All animal experiments were performed in accordance with protocols approved by the New York University Grossman School of Medicine Institutional Animal Care and Use Committee.

Bone marrow transduction and transplantation for generation of T-ALL

To generate the original GFP+ DKO and mCherry+ WT T-ALL lines, hematopoietic cells were isolated from bone marrow by flushing femurs and tibias. Stem and progenitor cells were enriched by magnetic selection of cells expressing c-Kit (STEMCELL EasySep Mouse Biotin Positive Selection Kit II). Cells were cultured in the presence of 50 ng/mL Flt3 ligand, 50 ng/mL stem cell factor (SCF), 10 ng/mL interleukin-3 (IL-3), and 10 ng/mL interleukin-6 (IL-6) (PeproTech) in OptiMEM + GlutaMAX (Invitrogen) supplemented with 10% fetal bovine serum (FBS)(Cytiva), 100 IU/mL penicillin and 100 ug/mL streptomycin (Gibco or Corning), and 55 μM β-mercaptoethanol (Sigma). 24 and 48 hr after enrichment, c-Kit+ cells were infected with retrovirus (MSCV Notch1ΔE-IRES-GFP[12] or Notch1ΔE-IRES-mCherry[12]), generated by transfection of Platinum E (Plat-E) retroviral packaging cells (Cell BioLabs Inc.), and concentrated by filtration according to the manufacturer's instructions (Amicon Ultra-15; 100,000 NMWL). Transduction efficiency was determined by reporter fluorescence at 96 hr. Irradiated C57BL/6 mice (two rounds of 500 rads) received 35 * 10^3 Notch1-ΔE-IRES-GFP/mCherry+, lineage− (lineage markers: CD4, CD8, B220, Gr1, Ter119, CD11b) cells, together with 500 * 10^3 unfractionated bone marrow cells for hemogenic support, intravenously by retro-orbital injection. Mice were bled regularly to monitor leukemia progression. The DKO donor hematopoietic cells were *Itgal*$^{-/-}$ *Itgb1*$^{f/f}$ *Mx1*-Cre. To delete *Itgb1*, when GFP+ blasts reached >10% of peripheral blood, mice received three intraperitoneal injections of poly(I:C) (10 ug/g, GE Heathcare) in PBS, administered every other day. Notch1ΔE-IRES-GFP *Itgb1*$^{f/f-}$ *Itgal*$^{-/-}$ *Mx1-cre* cells (DKO T-ALL) or Notch1ΔE-IRES-mCherry cells (WT T-ALL) were isolated from bone marrow at a humane endpoint.

For secondary model induction T-ALL cells were maintained *in vitro* (see below). For induction, recipients were sub-lethally irradiated (550 cGy) and retro-orbitally injected with 1–2 * 10^6 T-ALL cells. Radiation was performed with either Cs or X-ray irradiator (X-rad 320/350).

T-ALL cell culture

Primary mouse T-ALL cells isolated from bone marrow were maintained on OP9 stromal cells[61], kindly provided by Iannis Aifantis, in OptiMEM + GlutaMAX (Invitrogen) supplemented with 10% fetal bovine serum (FBS, Cytiva), 5 ng/ml IL-7, 100 IU/mL penicillin and 100 ug/mL streptomycin (Gibco or Corning), and 55 μM β-mercaptoethanol. Cells were passaged every 3–4 days onto a fresh feeder layer. OP9 cells were cultured in 75cm^2 flasks in MEMα + GlutaMAX (Invitrogen) supplemented with 20% FBS and 100 IU/mL penicillin and 100 ug/mL streptomycin (Gibco or Corning) and passaged every 2-3 days. For co-culture, OP9s were pre-treated with 7.5 ng/mL mitomycin C (Sigma) for 3-4 hours to prevent feeder cell division. T-ALL cells for leukemia induction were isolated from co-culture by density gradient (Ficoll-paque Premium, Cytiva). The same OP9 cell line was used for all experiments and DKO and WT T-ALL cells were always cultured on OP9 cells from the same flask and passaged the same number of times.

Retroviral transduction of T-ALL cells

The coding regions of *Itgb1* and *Itgal* (Dharmacon) were cloned into the pMXs-IRES-mCherry retroviral vector, and Plat-E packaging cells were used for the generation of retrovirus. DKO T-ALL cells, seeded on mitomycin C-treated OP9s, were transduced with a retrovirus encoding either *Itgb1* or *Itgal* or empty vector. 48-72 hours after transduction, cells were sorted on a BD FACSAria II for positive surface expression of αL or β1. Cells were allowed to recover on MMC-treated OP9s for 48 hours and another round of transduction was performed using the plasmid carrying the other gene. After 48-72 hours, T-ALL cells double-positive for surface expression of αL and β1 were sorted on the BD FACSAria II.

CRISPR deletion of genes in T-ALL cells

gRNAs targeting *Itgal*, *Itgb1* and *Itgb7* were ordered from IDT (sequences below) for use with the IDT Alt-R CRISPR-Cas9 system. ALT-R CRISPR-Cas9 Negative Control crRNA#1 was ordered as a non-targeting control (IDT). On day of nucleofection, gRNAs were resuspended in sterile tris-EDTA pH 8.0 to a concentration of 100uM. 1.2 uL of each gRNA for either *Itgal* or *Itgb1* or *Itgb7* were mixed with 1.7 uL of Alt-R S.p. HiFi Cas9 Nuclease V3, and 0.9 uL of PBS (total volume of 5 uL), and incubated for 20 minutes at room temperature, per manufacturer's instructions. 1-2*10^6 T-ALL cells were resuspended in 100uL P3 nucleofector solution (82 uL nucleofection solution + 18 uL supplement; Lonza P3 Primary Cell 4D-Nucleofector™ X Kit), combined with gRNA-Cas9 complex, and nucleofected using program "*activated T cells"* using the Lonza Amaxa 4D Nucleofector. Immediately after, 500 uL warm media was added to cells in cuvette and incubated for 10 min at 37C before cells were returned to culture. After 48-72 hours, T-ALL cells were sorted based on surface expression of αL or β1 on BD FACSAria II. T-ALL cells were then subjected to a second round to delete both *Itgal* and *Itgb1* and in some cases a third round to delete *Itgb7*.

Itgb1:
Mm.Cas9.ITBG1.1.AB: 5' ACA UUC UCC GCA AGA UUG UUU UAG AGC UAG AAA UAG CAA GUU AAA AUA AGG CUA GUC CGU UAU CAA CUU GAA AAA GUG GCA CCG AGU CGG UGC 3'
Mm.Cas9.ITBG1.1.AC: 5' GUC ACC AAU CGC AGC AAG UUU UAG AGC UAG AAA UAG CAA GUU AAA AUA AGG CUA GUC CGU UAU CAA CUU GAA AAA GUG GCA CCG AGU CGG UGC 3'

Itgal:
Mm.Cas9.ITGAL.1.AC: 5' GUA CUU GGG AAU GAC GCG UUU UAG AGC UAG AAA UAG CAA GUU AAA AUA AGG CUA GUC CGU UAU CAA CUU GAA AAA GUG GCA CCG AGU CGG UGC 3'
Mm.Cas9.ITGAL.1.AE: 5' GCC AAG AAG CUC UGC GUG UUU UAG AGC UAG AAA UAG CAA GUU AAA AUA AGG CUA GUC CGU UAU CAA CUU GAA AAA GUG GCA CCG AGU CGG UGC 3'

Itgb7:
Mm.Cas9.ITGB7.1.AA: 5' CAG CAC CGU UUU GUC CAC GAG UUU UAG AGC UAG AAA UAG CAA GUU AAA AUA AGG CUA GUC CGU UAU CAA CUU GAA AAA GUG GCA CCG AGU CGG UGC 3'
Mm.Cas9.ITGB7.1.AC: 5' CGU GGA CCU AUA UUA CCU UAG UUU UAG AGC UAG AAA UAG CAA GUU AAA AUA AGG CUA GUC CGU UAU CAA CUU GAA AAA GUG GCA CCG AGU CGG UGC 3'

Tissue isolation and processing for flow cytometry

All mice were euthanized and perfused with 5-10mL PBS. Unless otherwise specified, after isolation, all tissues and cell suspensions were stored in PBS/2% FBS on ice.
Blood: collected via cardiac puncture and stored in blood collection tube with K_2EDTA (BD Microtainer).
Bone marrow: right tibia and femur were flushed with PBS/2% FBS.
Skull bone marrow: isolated from calvarium by mechanical disruption with glass mortar and pestle.
Spleen and lymph nodes: mechanical disruption and filtration through a 100um cell strainer with the flat end of a 1mL syringe plunger.
Central nervous system (CNS): brain and inside of the dura attached to skull were washed with PBS/2% FBS via p1000 pipette and cells were collected. The wash and whole brain were placed in a 50mL conical tube and pulse-vortexed on low speed for 15 seconds. Brain was collected and mechanically disrupted and filtered through a 100um cell strainer with the flat end of a 1mL syringe plunger. Lymphocytes were purified by centrifugation using a 33% isotonic density gradient (Percoll; GE Healthcare). Red blood cells were depleted using tris-ammonium chloride solution. For later experiments (Fig. 2D-4), we determined that brain parenchyma processing was dispensable: >95% of T-ALL cells were collected with just wash of inside of dura and vortex of whole brain, and ratio was unaffected. All mice in each experiment were processed using the same protocol.
Cell counting: single-cell suspensions were counted using a Multisizer 3 (Beckman Coulter) set to detect nuclei between 3.5-10um. Total cell counts from bone marrow were obtained by assuming that cells isolated from tibia and femur of one leg represent 10% of the total bone marrow per mouse

(unless otherwise noted). Total cell counts from blood were obtained by assuming that the total amount of blood per mouse is 2mL.

Immunostaining and flow cytometry

Immunostaining: Unless otherwise specified, surface stains were performed on live cells with fluorophore-conjugated antibodies at 1:200 dilution in PBS supplemented with 2% FBS, 2% Normal Mouse Serum (NMS), and 2% Normal Rat Serum (NRS), for 20 minutes on ice and protected from light.

Antibodies purchased from Biolegend: anti-B220 (clone RA3-6B2), anti-CD4 (clone GK1.1), anti-CD8 (clone 53-6.7), anti-CD11a (clone M17/4), anti-CD11b (clone M1/70), anti-CD25 (clone PC61), anti-CD31 (clone MEC13.3), anti-CD44 (clone IM7), anti-CD45 (clone 30-F11), anti CD45.1 (clone A20), anti-CD45.2 (clone 104), anti-CD49d (clone R1-2), anti-CD104 (clone 346-11A), anti-β7 (clone FIB504), anti-CX3CR1 (SA011F11), anti-GR1 (clone RB6-8C5), anti-Ter119 (clone TER-119), Streptavidin, mouse IgG2a isotype control (clone MOPC-173) and rat IgG2a, k isotype control (clone RTK2758).

Antibodies purchased from eBioscience: anti-CD4 (clone GK1.5), anti-CD29 (clone eBioHMb1-1), anti-Lyve1 (clone ALY7), and Armenian Hamster IgG isotype control (clone eBio299Arm).

Apoptosis stains: anti-Active Caspase-3 (clone C92-605) was purchased from BD Biosciences and cells were fixed and permeabilized according to kit instructions (BD Biosciences Cytofix/Cytoperm Cat: BDB554714). Cells were stained at a concentration of 1:100 for 20 minutes at 4C.

Viability stains: "LIVE/DEAD™ Fixable Far Red Dead Cell Stain Kit, for 633 or 635 nm excitation" was purchased and used according to kit instructions (ThermoFisher).

EdU labelling: "Click-iT™ Plus EdU Alexa Fluor™ 488 Flow Cytometry Assay Kit" and "Click-iT™ Plus EdU Alexa Fluor™ 647 Flow Cytometry Assay Kit" were purchased and cells were stained according to kit instructions (ThermoFisher). DNA quantification was performed by staining with DAPI (Sigma) at 2ug/mL with 5ug/ml RNAse A (Thermo Scientific) for 15 minutes at RT.

Flow cytometry: data was acquired using a BD LSRII or Beckman Coulter Cytoflex using BD FACSDiva or Beckman Coulter CytExpert software. Data was analyzed using FlowJo v9 and v10.

Mouse treatments

For partial irradiation/shielding of CNS: 1/16" sheet lead (McMaster-Carr) was formed into a half cylinder (6" long, 2" radius) with two semi-circular cut outs in the middle of the long sides (approx. 1-1.5" deep). Four of these half-cylinders were nested to achieve a total thickness of ¼" inch lead and secured with tape. Mice were anesthetized with ketamine/xylazine (100mg/kg /10 mg/kg) and placed on a rigid, irradiator-safe surface with their limbs taped out perpendicular to their body. The lead shielding was placed over the mice, ensuring that their taped limbs were exposed by the semi-circular cut outs, and that all other parts of their body, including the tail, were underneath the lead. Mice were irradiated with 550 cGy using an X-ray irradiator with directional collimator and SnAlCu filter (X-rad320, Precision X-Ray).

For ablation of meningeal lymphatics, 5–8-week-old female C57BL/6 mice were injected intraperitoneally with $1*10^{12}$ PFU of either AAV-VEGFR3(1-4)-Ig (active) or AAV-VEGFR3(4-7)-Ig (control) (provided by Kari Alitalo).

For intraventricular infusion, mice were surgically implanted with an intraventricular cannula (P1 Technologies, C315GS-4/SP GUIDE 26GA 38834 4MM Pedestal, 2MM Projection) in the left lateral ventricle (-0.5mm R/C, -1.0mm M/L, -1.8mm D/V relative to bregma). For infusions, >5uL was drawn up into a 33G air-tight Hamilton Syringe (Hamilton, 1705 series) and syringe was mounted in a Remote Infuse/Withdraw Pump 11 Elite Nanomite Programmable Syringe Pump (Harvard Apparatus) mounted on a stereotaxic instrument (Model 940, Kopf). Mice were anesthetized with isoflurane (1.5%-2.5%) or ketamine/xylazine (100mg/kg / 10mg/kg) and mounted via bite bar/nose cone. Syringe needle was advanced into cannula 8.5mm from opening (approx. 0.3-0.5mm into lateral ventricle) and 5uL infusion was conducted at 250nL/min with a 10min rest before needle was withdrawn. *For dye infusion,* NHS-ester-Atto647 (Sigma) was dissolved in DMSO at 10mg/mL (stored at -20C), then further diluted 1:5 in PBS to 2mg/mL for infusions.

For myeloid cell depletion, CSF1R inhibitor PLX5622 was formulated at 1200ppm into rodent diet AIN-76A by Research Diets, Inc. (New Brunswick, NJ). Animals received either the PLX5622 formulated diet or a normal chow diet (AIN-76A) a week prior to leukemia induction and for the duration of the experiment (total four weeks). Both PLX5622 and control diet were irradiated and contained red dye.

For EdU labelling experiments, mice were administered 100ug EdU (ThermoFisher) in 100uL PBS intraperitoneally at 4h and 2h before euthanasia for a total dose of 200ug EdU.

For 5-fluorouracil experiments, 5-fluorouracil (5FU) (Sigma) was dissolved in DMSO to a concentration of 50mg/mL and stored at -20C. For injections, 5FU was diluted 1:10 in PBS to 5mg/mL and mice were injected intraperitoneally at a dose of 40mg/kg. Vehicle-treated mice were injected with 150uL of 10% DMSO/PBS.

For blocking antibody experiments, intracerebral ventricular infusions were performed as described above. Anti-CD49d (PS/2; Bio-Xcell) and anti-CD11a (M17/4; Bio-Xcell) were combined at equal quantities for a total of 26ug of each in 5uL. Isotype control mice received 5uL (47ug) of Rat IgG2a, anti-trinitrophenol (clone 2A3; Bio-Xcell). Infusions were performed three days and one day before tissue isolation and analysis.

Immunofluorescence

Meninges whole mounts, adapted from[70]. The top of the skull was removed with surgical scissors. While still attached to the skull, whole-mount meninges were fixed in 2% PFA overnight at 4C. The dura/arachnoid was then peeled from the skullcap. Meninges were incubated in blocking solution [PBS containing 2% normal serum (goat and/or donkey), 3% bovine serum albumin (BSA) (Fisher), anti-CD16/32 (clone 93, eBioscience, 1:1,000), 0.1% Triton X- 100, and 0.05% Tween 20] supplemented with avidin block (Vector Laboratories) for one hour at RT on a shaker; washed (with PBS 3 times for 5 min each at RT); followed by another one-hour block at RT with blocking buffer supplemented with biotin block (Vector Laboratories), and washed again. Primary antibodies were applied at 1:200 dilution in staining buffer [PBS containing 3% BSA and 0.5% Triton X-100] and meninges were incubated overnight at 4C. Meninges were washed then incubated in appropriate dilutions of secondary antibodies in staining buffer for 2 hours at RT or overnight at 4C. Meninges were washed, then wet mounted on a Superfrost Plus glass slide, and allowed to dry for 10-15 minutes. Fluoromount G and a coverslip were added and slides were allowed to fully dry at RT (16h) before edges were sealed with clear nail polish.

Primary antibodies: anti-Lyve-1 biotinylated (clone ALY7; eBioscience), anti-CD31-PE (clone MEC13.3; Biolegend), anti-GFP (ab13970; Abcam), anti-RFP (600-401-379, Rockland).

Secondary antibodies, Streptavidin-BV421 1:500 (Biolegend), Alexa Fluor 488 AffiniPure Goat Anti-Chicken IgY (IgG) (H+L) 1:1000 (Jackson ImmunoResearch), Alexa Fluor 647 AffiniPure Donkey Anti-Rabbit IgG (H+L) 1:1000 (Jackson ImmunoResearch), Cy3 Affinipure Donkey anti-Rabbit IgG (H+L) 1:1000 (Jackson ImmunoResearch).

Images were acquired using confocal microscope (LSM710 (Carl Zeiss) or Stellaris 8 (Leica)) with a 10x dry or 20x dry objective using ZEN (Zeiss) or LasX (Leica) software. Images were processed and analyzed using ImageJ (version 1.53; National Institutes of Health) and FIJI (version 2.14.0, Schindelin et al, 2012).

In vitro meningeal fibroblast assay

For meningeal fibroblast culture, dural meninges were isolated from naïve wild-type mice as described in (Louveau et al., 2015) and placed immediately in microcentrifuge tubes of digestion buffer containing collagenase D (1mg/ml, MilliporeSigma), DNAse I (50ug/mL, Roche), and Dispase (5 U/mL, Roche) in serum-free, high-glucose DMEM (Invitrogen) (modified from Remsik et al., 2021) and stored on ice. Tissues in microtubes were placed on rotator for 2h at 37C. Suspension was agitated by pipetting until fully dissociated and filtered through 40um cell strainer. Single cell suspension was pelleted at 400g for 4m and seeded on 6-well tissue culture treated plates in meningeal fibroblast media (high-glucose

DMEM supplemented with 15% FBS (Cytiva) and 100 IU/mL penicillin and 100 ug/mL streptomycin (Gibco or Corning)). 16h after seeding, media and non-attached cell fraction was aspirated, leaving fibroblasts behind, and media was replaced and changed every 2-3 days. Meningeal fibroblasts were cultured for 10-14 days and passaged into 12-well plates twice before *in vitro* assay.
For assay, DKO and WT T-ALL were isolated from culture by density gradient (as described above). T-ALL cells were combined at a ratio of 1:1 and plated on either mitomycin-treated OP9s (as above) or meningeal fibroblasts from naïve mice in 12 well plates at 50,000-100,000 T-ALL cells/well. After 3 days, T-ALL cells were collected by trypsinization and analyzed.
For in vitro EdU labelling, culture was performed as above; 1 hour before T-ALL was isolated, 10mM EdU was added to the media. EdU staining was performed per manufacturer's directions (as above).

RNA extraction and sequencing
CRISPR-DKO and CRISPR-WT (both CD45.2) cells were isolated from the CNS and spleen of 1:1 DKO:WT co-transfer mice (congenically-marked,CD45.1/.2) at mid-stage disease, stained for the presence of the integrins and CD45.1 and CD45.2, and sorted using a BD FACS Aria.

Total RNA was extracted using RNeasy Plus Micro Kit (Qiagen) and purified with RNAse-Free DNAse (Qiagen). Total RNA was quantified on an Agilent BioAnalyzer via the Pico kit (Agilent). SMART-Seq HT Kit (Takara) was used to construct cDNA and libraries. cDNA was constructed using 1ng input of RNA and amplified with 12 cycles. cDNA product was purified with DNA AMPure beads (Beckman-Coulter) and quantified via Agilent Quant-IT. 300pg of each cDNA sample was used to construct libraries via Nextera XT DNA library preparation kit. 12 PCR cycles were used to amplify the libraries and to add the barcodes. Libraries were then cleaned, quantified, and pooled for sequencing on an S1 (100 cycles) flow cell on Illumina NovaSeq sequencer.

Sequencing reads were mapped to the reference genome (mm10) using the STAR aligner (v2.5.0c)[65]. Alignments were guided by a Gene Transfer Format (GTF) file. The mean read insert sizes and their standard deviations were calculated using Picard tools (v.1.126) (http://broadinstitute.github.io/picard). The read count tables were generated using HTSeq (v0.6.0)[66], normalized based on their library size factors using DEseq2[67], and differential expression analysis was performed. The Read Per Million (RPM) normalized BigWig files were generated using BEDTools (v2.17.0)[68] and bedGraphToBigWig tool (v4). All the downstream statistical analyses and generating plots were performed in R environment (v4.4) (https://www.r-project.org/) and RStudio (v 2024.04.0+735). Packages used to generate plots include TidyVerse[71] and GSEA was performed using DAVID[72,73] and visualized using ComplexHeatMap and circlize. [69]

Statistical analysis
Statistical analysis (excluding RNA-seq experiments) was conducted using the PRISM program (GraphPad). Experiments comparing the total number of WT to the total number of DKO T-ALL cells, and experiments comparing the ratio of DKO:WT between groups, were analyzed using a two-tailed, unpaired t-test with Welch's correction. Experiments comparing the survival or proliferation of WT to DKO T-ALL cells were analyzed using a two-tailed, paired t-test. For data displayed on a log-scale, $\log_{10}$-transformed data was used to calculate significance. For data presented as percentages, logit-transformed data was used to calculate significance. Significance was defined as $*p < 0.05$, $**p < 0.01$, $***p < 0.001$, $****p < 0.0001$.

References

1. Cronin, K.A., Scott, S., Firth, A.U., Sung, H., Henley, S.J., Sherman, R.L., Siegel, R.L., Anderson, R.N., Kohler, B.A., Benard, V.B., et al. (2022). Annual report to the nation on the status of cancer, part 1: National cancer statistics. Cancer *128*, 4251-4284. 10.1002/cncr.34479.
2. Inaba, H., and Pui, C.H. (2021). Advances in the Diagnosis and Treatment of Pediatric Acute Lymphoblastic Leukemia. J Clin Med *10*. 10.3390/jcm10091926.

3. Thastrup, M., Duguid, A., Mirian, C., Schmiegelow, K., and Halsey, C. (2022). Central nervous system involvement in childhood acute lymphoblastic leukemia: challenges and solutions. Leukemia *36*, 2751-2768. 10.1038/s41375-022-01714-x.
4. Frishman-Levy, L., and Izraeli, S. (2017). Advances in understanding the pathogenesis of CNS acute lymphoblastic leukaemia and potential for therapy. Br J Haematol *176*, 157-167. 10.1111/bjh.14411.
5. Hunger, S.P., and Mullighan, C.G. (2015). Acute Lymphoblastic Leukemia in Children. N Engl J Med *373*, 1541-1552. 10.1056/NEJMra1400972.
6. Pui, C.H., and Howard, S.C. (2008). Current management and challenges of malignant disease in the CNS in paediatric leukaemia. Lancet Oncol *9*, 257-268. 10.1016/S1470-2045(08)70070-6.
7. Engelhardt, B., and Ransohoff, R.M. (2012). Capture, crawl, cross: the T cell code to breach the blood–brain barriers. Trends in immunology *33*, 579-589.
8. Yednock, T.A., Cannon, C., Fritz, L.C., Sanchez-Madrid, F., Steinman, L., and Karin, N. (1992). Prevention of experimental autoimmune encephalomyelitis by antibodies against alpha 4 beta 1 integrin. Nature *356*, 63-66.
9. Baron, J.L., Madri, J.A., Ruddle, N.H., Hashim, G., and Janeway, C.A., Jr. (1993). Surface expression of alpha 4 integrin by CD4 T cells is required for their entry into brain parenchyma. The Journal of experimental medicine *177*, 57-68.
10. Rudick, R., Polman, C., Clifford, D., Miller, D., and Steinman, L. (2013). Natalizumab: bench to bedside and beyond. JAMA Neurol *70*, 172-182. 10.1001/jamaneurol.2013.598.
11. Yao, H., Price, T.T., Cantelli, G., Ngo, B., Warner, M.J., Olivere, L., Ridge, S.M., Jablonski, E.M., Therrien, J., and Tannheimer, S. (2018). Leukaemia hijacks a neural mechanism to invade the central nervous system. Nature *560*, 55-60.
12. Pitt, Lauren A., Tikhonova, Anastasia N., Hu, H., Trimarchi, T., King, B., Gong, Y., Sanchez-Martin, M., Tsirigos, A., Littman, Dan R., Ferrando, Adolfo A., et al. (2015). CXCL12-Producing Vascular Endothelial Niches Control Acute T Cell Leukemia Maintenance. Cancer Cell *27*, 755-768. https://doi.org/10.1016/j.ccell.2015.05.002.
13. Liu, Y., Easton, J., Shao, Y., Maciaszek, J., Wang, Z., Wilkinson, M.R., McCastlain, K., Edmonson, M., Pounds, S.B., Shi, L., et al. (2017). The genomic landscape of pediatric and young adult T-lineage acute lymphoblastic leukemia. Nat Genet *49*, 1211-1218. 10.1038/ng.3909.
14. Weng, A.P., Ferrando, A.A., Lee, W., Morris, J.P.t., Silverman, L.B., Sanchez-Irizarry, C., Blacklow, S.C., Look, A.T., and Aster, J.C. (2004). Activating mutations of NOTCH1 in human T cell acute lymphoblastic leukemia. Science *306*, 269-271. 10.1126/science.1102160.
15. Pear, W.S., Aster, J.C., Scott, M.L., Hasserjian, R.P., Soffer, B., Sklar, J., and Baltimore, D. (1996). Exclusive development of T cell neoplasms in mice transplanted with bone marrow expressing activated Notch alleles. The Journal of experimental medicine *183*, 2283-2291.
16. Ding, Z.M., Babensee, J.E., Simon, S.I., Lu, H., Perrard, J.L., Bullard, D.C., Dai, X.Y., Bromley, S.K., Dustin, M.L., Entman, M.L., et al. (1999). Relative contribution of LFA-1 and Mac-1 to neutrophil adhesion and migration. J Immunol *163*, 5029-5038.
17. Raghavan, S., Bauer, C., Mundschau, G., Li, Q., and Fuchs, E. (2000). Conditional Ablation of β1 Integrin in Skin. J. Cell Biol. *150*, 1149-1160. 10.1083/jcb.150.5.1149.
18. Luo, B.H., Carman, C.V., and Springer, T.A. (2007). Structural basis of integrin regulation and signaling. Annu Rev Immunol *25*, 619-647. 10.1146/annurev.immunol.25.022106.141618.
19. Yao, H., Price, T.T., Cantelli, G., Ngo, B., Warner, M.J., Olivere, L., Ridge, S.M., Jablonski, E.M., Therrien, J., Tannheimer, S., et al. (2018). Leukaemia hijacks a neural mechanism to invade the central nervous system. Nature *560*, 55-60. 10.1038/s41586-018-0342-5.
20. Berlin, C., Berg, E.L., Briskin, M.J., Andrew, D.P., Kilshaw, P.J., Holzmann, B., Weissman, I.L., Hamann, A., and Butcher, E.C. (1993). Alpha 4 beta 7 integrin mediates lymphocyte binding to the mucosal vascular addressin MAdCAM-1. Cell *74*, 185-195. 10.1016/0092-8674(93)90305-a.
21. Meeker, R.B., Williams, K., Killebrew, D.A., and Hudson, L.C. (2012). Cell trafficking through the choroid plexus. Cell adhesion & migration *6*, 390-396.
22. Rossi, B., Dusi, S., Angelini, G., Bani, A., Lopez, N., Della Bianca, V., Pietronigro, E.C., Zenaro, E., Zocco, C., and Constantin, G. (2023). Alpha4 beta7 integrin controls Th17 cell trafficking in

the spinal cord leptomeninges during experimental autoimmune encephalomyelitis. Front Immunol *14*, 1071553. 10.3389/fimmu.2023.1071553.
23. Zohren, F., Toutzaris, D., Klärner, V., Hartung, H.P., Kieseier, B., and Haas, R. (2008). The monoclonal anti-VLA-4 antibody natalizumab mobilizes CD34+ hematopoietic progenitor cells in humans. Blood *111*, 3893-3895. 10.1182/blood-2007-10-120329.
24. Papayannopoulou, T., Craddock, C., Nakamoto, B., Priestley, G.V., and Wolf, N.S. (1995). The VLA4/VCAM-1 adhesion pathway defines contrasting mechanisms of lodgement of transplanted murine hemopoietic progenitors between bone marrow and spleen. Proc Natl Acad Sci U S A *92*, 9647-9651. 10.1073/pnas.92.21.9647.
25. Bonig, H., Wundes, A., Chang, K.H., Lucas, S., and Papayannopoulou, T. (2008). Increased numbers of circulating hematopoietic stem/progenitor cells are chronically maintained in patients treated with the CD49d blocking antibody natalizumab. Blood *111*, 3439-3441. 10.1182/blood-2007-09-112052.
26. Louveau, A., Smirnov, I., Keyes, T.J., Eccles, J.D., Rouhani, S.J., Peske, J.D., Derecki, N.C., Castle, D., Mandell, J.W., and Lee, K.S. (2015). Structural and functional features of central nervous system lymphatic vessels. Nature *523*, 337-341.
27. Aspelund, A., Antila, S., Proulx, S.T., Karlsen, T.V., Karaman, S., Detmar, M., Wiig, H., and Alitalo, K. (2015). A dural lymphatic vascular system that drains brain interstitial fluid and macromolecules. Journal of Experimental Medicine *212*, 991-999.
28. Hunter, M.C., Teijeira, A., and Halin, C. (2016). T cell trafficking through lymphatic vessels. Frontiers in immunology *7*, 613.
29. Teijeira, A., Hunter, M.C., Russo, E., Proulx, S.T., Frei, T., Debes, G.F., Coles, M., Melero, I., Detmar, M., Rouzaut, A., and Halin, C. (2017). T Cell Migration from Inflamed Skin to Draining Lymph Nodes Requires Intralymphatic Crawling Supported by ICAM-1/LFA-1 Interactions. Cell Reports *18*, 857-865. 10.1016/j.celrep.2016.12.078 PMID - 28122237.
30. Antila, S., Karaman, S., Nurmi, H., Airavaara, M., Voutilainen, M.H., Mathivet, T., Chilov, D., Li, Z., Koppinen, T., and Park, J.-H. (2017). Development and plasticity of meningeal lymphatic vessels. Journal of Experimental Medicine *214*, 3645-3667.
31. Dustin, M.L. (2014). The immunological synapse. Cancer Immunol Res *2*, 1023-1033. 10.1158/2326-6066.cir-14-0161.
32. Li, Y., Yang, X., Sun, Y., Li, Z., Yang, W., Ju, B., Easton, J., Pei, D., Cheng, C., Lee, S., et al. (2022). Impact of T-cell immunity on chemotherapy response in childhood acute lymphoblastic leukemia. Blood *140*, 1507-1521. 10.1182/blood.2021014495.
33. Zamora, A.E., Crawford, J.C., Allen, E.K., Guo, X.J., Bakke, J., Carter, R.A., Abdelsamed, H.A., Moustaki, A., Li, Y., Chang, T.C., et al. (2019). Pediatric patients with acute lymphoblastic leukemia generate abundant and functional neoantigen-specific CD8. Sci Transl Med *11*. 10.1126/scitranslmed.aat8549.
34. Lyu, A., Triplett, T.A., Nam, S.H., Hu, Z., Arasappan, D., Godfrey, W.H., Ames, R.Y., Sarang, A., Selden, H.J., Lee, C.-H., et al. (2020). Tumor-associated myeloid cells provide critical support for T-ALL. Blood *136*, 1837-1850. 10.1182/blood.2020007145.
35. Lyu, A., Humphrey, R.S., Nam, S.H., Durham, T.A., Hu, Z., Arasappan, D., Horton, T.M., and Ehrlich, L.I.R. (2023). Integrin signaling is critical for myeloid-mediated support of T-cell acute lymphoblastic leukemia. Nat Commun *14*, 6270. 10.1038/s41467-023-41925-z.
36. Spangenberg, E., Severson, P.L., Hohsfield, L.A., Crapser, J., Zhang, J., Burton, E.A., Zhang, Y., Spevak, W., Lin, J., Phan, N.Y., et al. (2019). Sustained microglial depletion with CSF1R inhibitor impairs parenchymal plaque development in an Alzheimer's disease model. Nature Communications *10*, 3758. 10.1038/s41467-019-11674-z.
37. Lei, F., Cui, N., Zhou, C., Chodosh, J., Vavvas, D.G., and Paschalis, E.I. (2020). CSF1R inhibition by a small-molecule inhibitor is not microglia specific; affecting hematopoiesis and the function of macrophages. Proc National Acad Sci *117*, 23336-23338. 10.1073/pnas.1922788117.
38. Montilla, A., Zabala, A., Er-Lukowiak, M., Rissiek, B., Magnus, T., Rodriguez-Iglesias, N., Sierra, A., Matute, C., and Domercq, M. (2023). Microglia and meningeal macrophages depletion

delays the onset of experimental autoimmune encephalomyelitis. Cell Death Dis *14*, 16. 10.1038/s41419-023-05551-3.
39. Schläger, C., Körner, H., Krueger, M., Vidoli, S., Haberl, M., Mielke, D., Brylla, E., Issekutz, T., Cabañas, C., Nelson, P.J., et al. (2016). Effector T-cell trafficking between the leptomeninges and the cerebrospinal fluid. Nature *530*, 349-353. 10.1038/nature16939.
40. Derk, J., Jones, H.E., Como, C., Pawlikowski, B., and Siegenthaler, J.A. (2021). Living on the Edge of the CNS: Meninges Cell Diversity in Health and Disease. Front Cell Neurosci *15*, 703944. 10.3389/fncel.2021.703944.
41. Remsik, J., Saadeh, F., Tong, X., Li, M.J., Snyder, J., Bale, T., Wu, J., Derderian, C., Guber, D., Chi, Y., et al. (2021). Characterization, isolation, and in vitro culture of leptomeningeal fibroblasts. J Neuroimmunol *361*, 577727. 10.1016/j.jneuroim.2021.577727.
42. DeSisto, J., O'Rourke, R., Jones, H.E., Pawlikowski, B., Malek, A.D., Bonney, S., Guimiot, F., Jones, K.L., and Siegenthaler, J.A. (2020). Single-Cell Transcriptomic Analyses of the Developing Meninges Reveal Meningeal Fibroblast Diversity and Function. Developmental Cell *54*, 43-59.e44. https://doi.org/10.1016/j.devcel.2020.06.009.
43. Davidson, S., Coles, M., Thomas, T., Kollias, G., Ludewig, B., Turley, S., Brenner, M., and Buckley, C.D. (2021). Fibroblasts as immune regulators in infection, inflammation and cancer. Nat Rev Immunol *21*, 704-717. 10.1038/s41577-021-00540-z.
44. Buechler, M.B., and Turley, S.J. (2018). A short field guide to fibroblast function in immunity. Semin Immunol *35*, 48-58. 10.1016/j.smim.2017.11.001.
45. Cavagnero, K.J., and Gallo, R.L. (2022). Essential immune functions of fibroblasts in innate host defense. Front Immunol *13*, 1058862. 10.3389/fimmu.2022.1058862.
46. Bautista-Hernández, L.A., Gómez-Olivares, J.L., Buentello-Volante, B., and Bautista-de Lucio, V.M. (2017). Fibroblasts: The Unknown Sentinels Eliciting Immune Responses Against Microorganisms. Eur J Microbiol Immunol (Bp) *7*, 151-157. 10.1556/1886.2017.00009.
47. Mao, X., Xu, J., Wang, W., Liang, C., Hua, J., Liu, J., Zhang, B., Meng, Q., Yu, X., and Shi, S. (2021). Crosstalk between cancer-associated fibroblasts and immune cells in the tumor microenvironment: new findings and future perspectives. Molecular Cancer *20*, 131. 10.1186/s12943-021-01428-1.
48. Rustenhoven, J., Drieu, A., Mamuladze, T., Lima, K.A.d., Dykstra, T., Wall, M., Papadopoulos, Z., Kanamori, M., Salvador, A.F., Baker, W., et al. (2021). Functional characterization of the dural sinuses as a neuroimmune interface. Cell *184*, 1000-1016.e1027. 10.1016/j.cell.2020.12.040.
49. Rua, R., and McGavern, D.B. (2018). Advances in Meningeal Immunity. Trends Mol Med *24*, 542-559. 10.1016/j.molmed.2018.04.003.
50. Ramaglia, V., Florescu, A., Zuo, M., Sheikh-Mohamed, S., and Gommerman, J.L. (2021). Stromal Cell-Mediated Coordination of Immune Cell Recruitment, Retention, and Function in Brain-Adjacent Regions. J Immunol *206*, 282-291. 10.4049/jimmunol.2000833.
51. Ko, S.Y., Park, C.J., Park, S.H., Cho, Y.U., Jang, S., Seo, E.J., Kim, N., Kim, D.Y., Koh, K.N., Im, H.J., et al. (2014). High CXCR4 and low VLA-4 expression predicts poor survival in adults with acute lymphoblastic leukemia. Leuk Res *38*, 65-70. 10.1016/j.leukres.2013.10.016.
52. Shalapour, S., Hof, J., Kirschner-Schwabe, R., Bastian, L., Eckert, C., Prada, J., Henze, G., von Stackelberg, A., and Seeger, K. (2011). High VLA-4 expression is associated with adverse outcome and distinct gene expression changes in childhood B-cell precursor acute lymphoblastic leukemia at first relapse. Haematologica *96*, 1627-1635. 10.3324/haematol.2011.047993.
53. Cleaver, A.L., Beesley, A.H., Firth, M.J., Sturges, N.C., O'Leary, R.A., Hunger, S.P., Baker, D.L., and Kees, U.R. (2010). Gene-based outcome prediction in multiple cohorts of pediatric T-cell acute lymphoblastic leukemia: a Children's Oncology Group study. Mol Cancer *9*, 105. 10.1186/1476-4598-9-105.
54. Hsieh, Y.T., Gang, E.J., Geng, H., Park, E., Huantes, S., Chudziak, D., Dauber, K., Schaefer, P., Scharman, C., Shimada, H., et al. (2013). Integrin alpha4 blockade sensitizes drug resistant pre-B acute lymphoblastic leukemia to chemotherapy. Blood *121*, 1814-1818. 10.1182/blood-2012-01-406272.

55. Ruan, Y., Kim, H.N., Ogana, H.A., Gang, E.J., Li, S., Liu, H.-C., Bhojwani, D., Wayne, A.S., Yang, M., and Kim, Y.-M. (2022). In vitro and in vivo effects of AVA4746, a novel competitive antagonist of the ligand binding of VLA-4, in B-cell acute lymphoblastic leukemia. Exp. Ther. Med. *23*, 47. 10.3892/etm.2021.10969.
56. Berrazouane, S., Boisvert, M., Salti, S., Mourad, W., Al-Daccak, R., Barabé, F., and Aoudjit, F. (2019). Beta1 integrin blockade overcomes doxorubicin resistance in human T-cell acute lymphoblastic leukemia. Cell Death & Disease *10*, 357. 10.1038/s41419-019-1593-2.
57. Hsieh, Y.T., Gang, E.J., Shishido, S.N., Kim, H.N., Pham, J., Khazal, S., Osborne, A., Esguerra, Z.A., Kwok, E., Jang, J., et al. (2014). Effects of the small-molecule inhibitor of integrin α4, TBC3486, on pre-B-ALL cells. Leukemia *28*, 2101-2104. 10.1038/leu.2014.182.
58. Matsunaga, T., Takemoto, N., Sato, T., Takimoto, R., Tanaka, I., Fujimi, A., Akiyama, T., Kuroda, H., Kawano, Y., Kobune, M., et al. (2003). Interaction between leukemic-cell VLA-4 and stromal fibronectin is a decisive factor for minimal residual disease of acute myelogenous leukemia. Nat. Med. *9*, 1158-1165. 10.1038/nm909.
59. Winter, S.S., Sweatman, J.J., Lawrence, M.B., Rhoades, T.H., Hart, A.L., and Larson, R.S. (2001). Enhanced T-lineage acute lymphoblastic leukaemia cell survival on bone marrow stroma requires involvement of LFA-1 and ICAM-1. Br J Haematol *115*, 862-871. 10.1046/j.1365-2141.2001.03182.x.
60. Talamonti, M., Spallone, G., Di Stefani, A., Costanzo, A., and Chimenti, S. (2011). Efalizumab. Expert Opinion on Drug Safety *10*, 239-251. 10.1517/14740338.2011.524925.
61. Nakano, T., Kodama, H., and Honjo, T. (1994). Generation of lymphohematopoietic cells from embryonic stem cells in culture. Science *265*, 1098-1101. 10.1126/science.8066449.
62. Kühn, R., Schwenk, F., Aguet, M., and Rajewsky, K. (1995). Inducible Gene Targeting in Mice. Science *269*, 1427-1429. 10.1126/science.7660125.
63. Pearson, T., Shultz, L.D., Miller, D., King, M., Laning, J., Fodor, W., Cuthbert, A., Burzenski, L., Gott, B., Lyons, B., et al. (2008). Non-obese diabetic–recombination activating gene-1 (NOD–Rag 1 null) interleukin (IL)-2 receptor common gamma chain (IL 2 rγnull) null mice: a radioresistant model for human lymphohaematopoietic engraftment. Clin. Exp. Immunol. *154*, 270-284. 10.1111/j.1365-2249.2008.03753.x.
64. Mäkinen, T., Jussila, L., Veikkola, T., Karpanen, T., Kettunen, M.I., Pulkkanen, K.J., Kauppinen, R., Jackson, D.G., Kubo, H., Nishikawa, S.-I., et al. (2001). Inhibition of lymphangiogenesis with resulting lymphedema in transgenic mice expressing soluble VEGF receptor-3. Nat. Med. *7*, 199-205. 10.1038/84651.
65. Dobin, A., Davis, C.A., Schlesinger, F., Drenkow, J., Zaleski, C., Jha, S., Batut, P., Chaisson, M., and Gingeras, T.R. (2013). STAR: ultrafast universal RNA-seq aligner. Bioinformatics *29*, 15-21. 10.1093/bioinformatics/bts635.
66. Anders, S., Pyl, P.T., and Huber, W. (2015). HTSeq--a Python framework to work with high-throughput sequencing data. Bioinformatics *31*, 166-169. 10.1093/bioinformatics/btu638.
67. Love, M.I., Huber, W., and Anders, S. (2014). Moderated estimation of fold change and dispersion for RNA-seq data with DESeq2. Genome Biol *15*, 550. 10.1186/s13059-014-0550-8.
68. Quinlan, A.R., and Hall, I.M. (2010). BEDTools: a flexible suite of utilities for comparing genomic features. Bioinformatics *26*, 841-842. 10.1093/bioinformatics/btq033.
69. Gu, Z., Gu, L., Eils, R., Schlesner, M., and Brors, B. (2014). circlize implements and enhances circular visualization in R. Bioinformatics *30*, 2811-2812. 10.1093/bioinformatics/btu393.
70. Louveau, A., Herz, J., Alme, M.N., Salvador, A.F., Dong, M.Q., Viar, K.E., Herod, S.G., Knopp, J., Setliff, J.C., and Lupi, A.L. (2018). CNS lymphatic drainage and neuroinflammation are regulated by meningeal lymphatic vasculature. Nature neuroscience *21*, 1380-1391.
71. Wickham H, A.M., Bryan J, Chang W, McGowan LD, François R,, Grolemund G, H.A., Henry L, Hester J, Kuhn M, Pedersen TL, Miller E,, Bache SM, M.K., Ooms J, Robinson D, Seidel DP, Spinu V, Takahashi K,, and Vaughan D, W.C., Woo K, Yutani H (2019). Welcome to the tidyverse.
72. Sherman, B.T., Hao, M., Qiu, J., Jiao, X., Baseler, M.W., Lane, H.C., Imamichi, T., and Chang, W. (2022). DAVID: a web server for functional enrichment analysis and functional annotation of gene lists (2021 update). Nucleic Acids Res *50*, W216-w221. 10.1093/nar/gkac194.

73. Huang da, W., Sherman, B.T., and Lempicki, R.A. (2009). Systematic and integrative analysis of large gene lists using DAVID bioinformatics resources. Nat Protoc *4*, 44-57. 10.1038/nprot.2008.211.

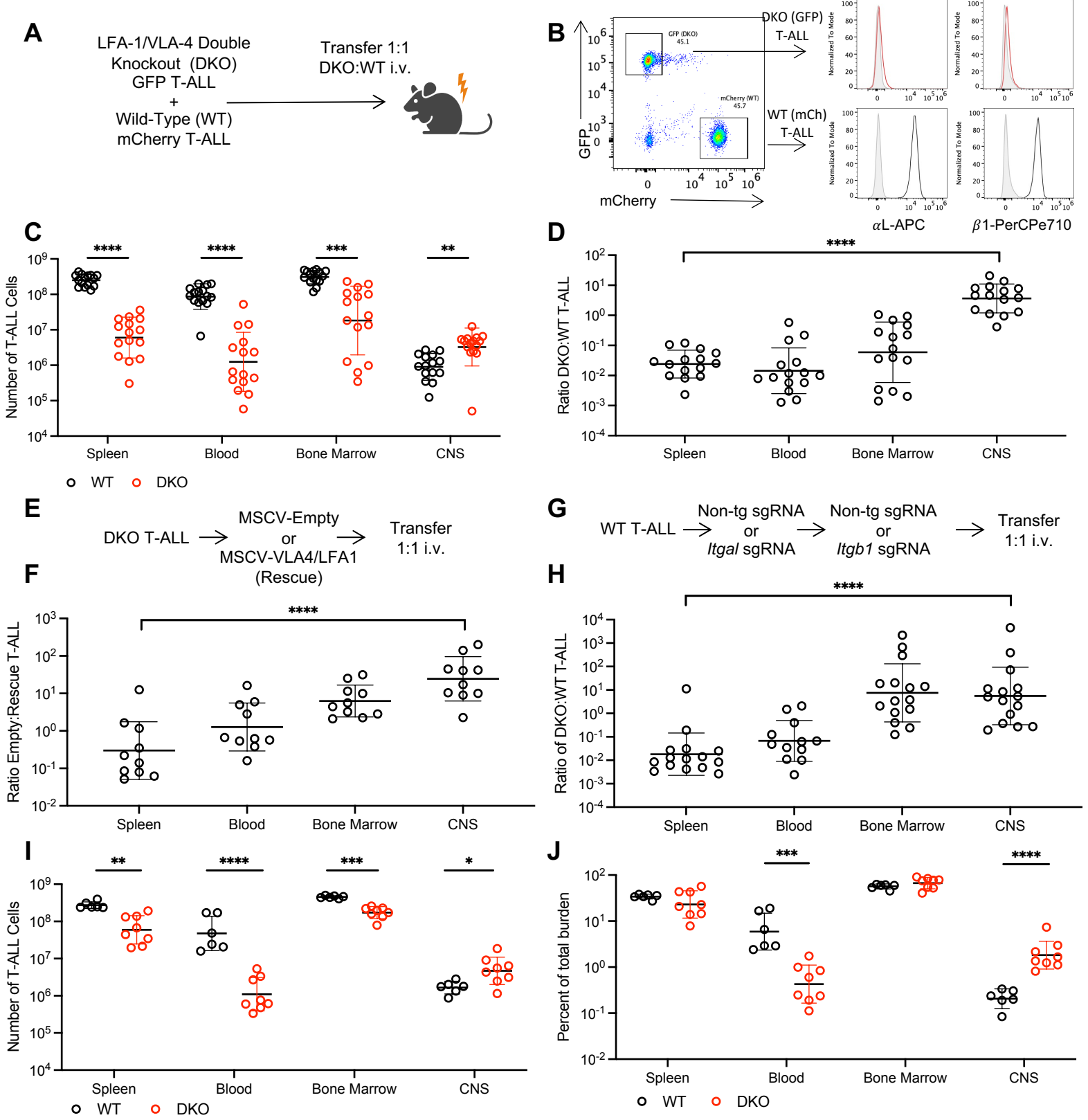

Fig. 1. Integrin-deficient T-ALL accumulates in the central nervous system compared to WT T-ALL.
(A-D) WT NOTCH1-ΔE mCherry⁺ T-ALL and DKO NOTCH1-ΔE GFP⁺ T-ALL cells were mixed 1:1 and transferred intravenously (i.v.) into sub-lethally irradiated recipients. **(A)** Experiment design. **(B)** Left: Representative flow cytometry plot distinguishing WT T-ALL and DKO T-ALL from the CNS. Right: Representative surface stain of β1 and αL integrins on T-ALL. Black: WT, red: DKO, grey: isotype. Numbers **(C)** and ratios **(D)** of DKO (red) and WT (black) T-ALL cells found in the indicated tissues at a humane endpoint. Data compiled from 3 experiments; *n* = 15. **(E-F)** DKO T-ALL cells were transduced with either vectors encoding *Itgal* and *Itgb1* ("rescue") or empty vector ("empty") and transferred 1:1 i.v. into sub-lethally irradiated recipients. **(E)** Experiment design. **(F)** Ratio of DKO-empty to DKO-rescue T-ALL cells in the indicated tissues at a humane endpoint. Data compiled from two experiments; *n* = 10.
(G-H) WT T-ALL cells were nucleofected with sgRNAs targeting *Itgal* or non-targeting gRNAs along with recombinant Cas9 protein. The process was repeated for *Itgb1* to generate "CRISPR-DKO" and "CRISPR-WT T-ALL." The cells were mixed 1:1 and transferred i.v. into sub-lethally irradiated recipients. **(G)** Experiment design. **(H)** Ratio of CRISPR-DKO to CRISPR-WT T-ALL cells found in the indicated tissues at a humane endpoint. Data compiled from five experiments; *n* = 15. **(I-J)** Sub-lethally irradiated WT mice received either WT or DKO T-ALL i.v. Number **(I)** or relative disease burden **(J)** of DKO (red; *n* = 8) or WT (black; *n* = 6) T-ALL cells found in the indicated tissues at a humane endpoint. Data compiled from 2 experiments. Bars represent geometric mean and geometric SD. Statistics calculated on log-transformed data using unpaired t-test with Welch's correction. *p ≤ 0.05, **p ≤ 0.01, ***p ≤ 0.001, ****p ≤ 0.0001

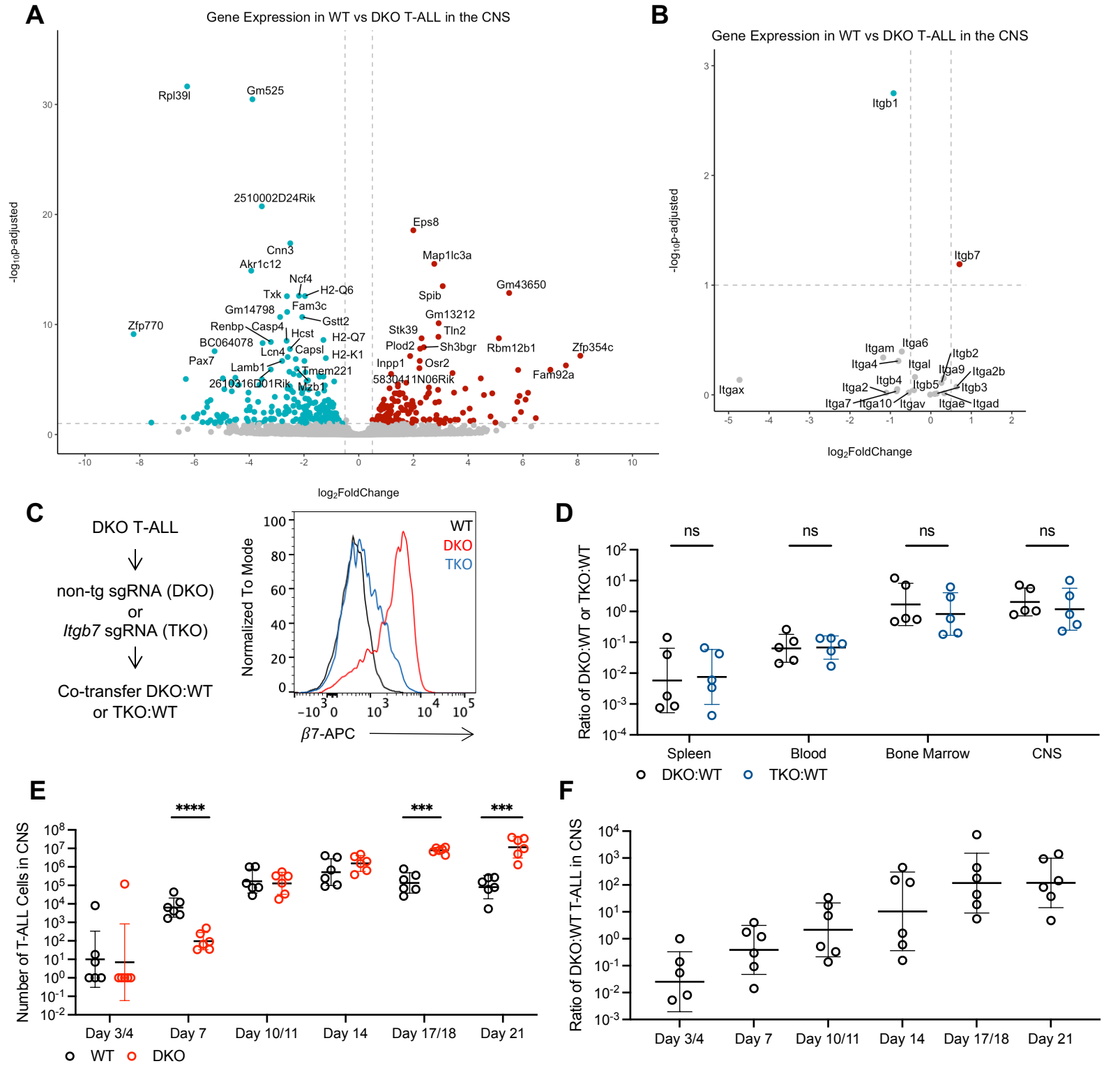

Fig. 2. Integrin-deficient T-ALL is unlikely to accumulate in the CNS due to enhanced entry.
(A, B) RNA-Sequencing was performed on CRISPR-WT and CRISPR-DKO T-ALL cells isolated from the CNS of mice at mid-stage disease that had received 1:1 DKO:WT T-ALL. Volcano plots of **(A)** all differentially expressed genes or **(B)** integrin-family genes. (Right, red) genes that are upregulated in the DKO T-ALL; (Left, blue) genes that are downregulated in the DKO T-ALL. Vertical lines represent log2FoldChange = -0.5, 0.5; horizontal line represents FDR = 0.1. Residual *Itgal* and *Itgb1* expression likely reflects truncated transcripts, as no surface protein remains. Average of $n = 4$ biological replicates. Statistics calculated using DESeq2 and corrected for multiple comparisons.
(C) Left, CRISPR-TKO T-ALL generation. Right, representative surface staining of integrin β7 on T-ALL cells (blue: TKO, black: WT, red: DKO).
(D) Ratio of DKO:WT T-ALL (black; $n = 5$) or TKO:WT T-ALL (blue; $n = 5$) in indicated tissues at a humane endpoint. Data compiled from two experiments.
(E, F) Sub-lethally irradiated WT mice were injected i.v. with 1:1 DKO:WT T-ALL and tissues were isolated from 3 mice every 3-4 days. **(E)** Total number of WT (black) and DKO (red) T-ALL cells in the CNS. **(F)** Ratio of DKO:WT T-ALL in the CNS. Data compiled from two experiments; $n = 36$.
Bars represent geometric mean and geometric SD. Statistics calculated on log-transformed data using unpaired t-test with Welch's correction. *$p \leq 0.05$, **$p \leq 0.01$, ***$p \leq 0.001$, ****$p \leq 0.0001$.

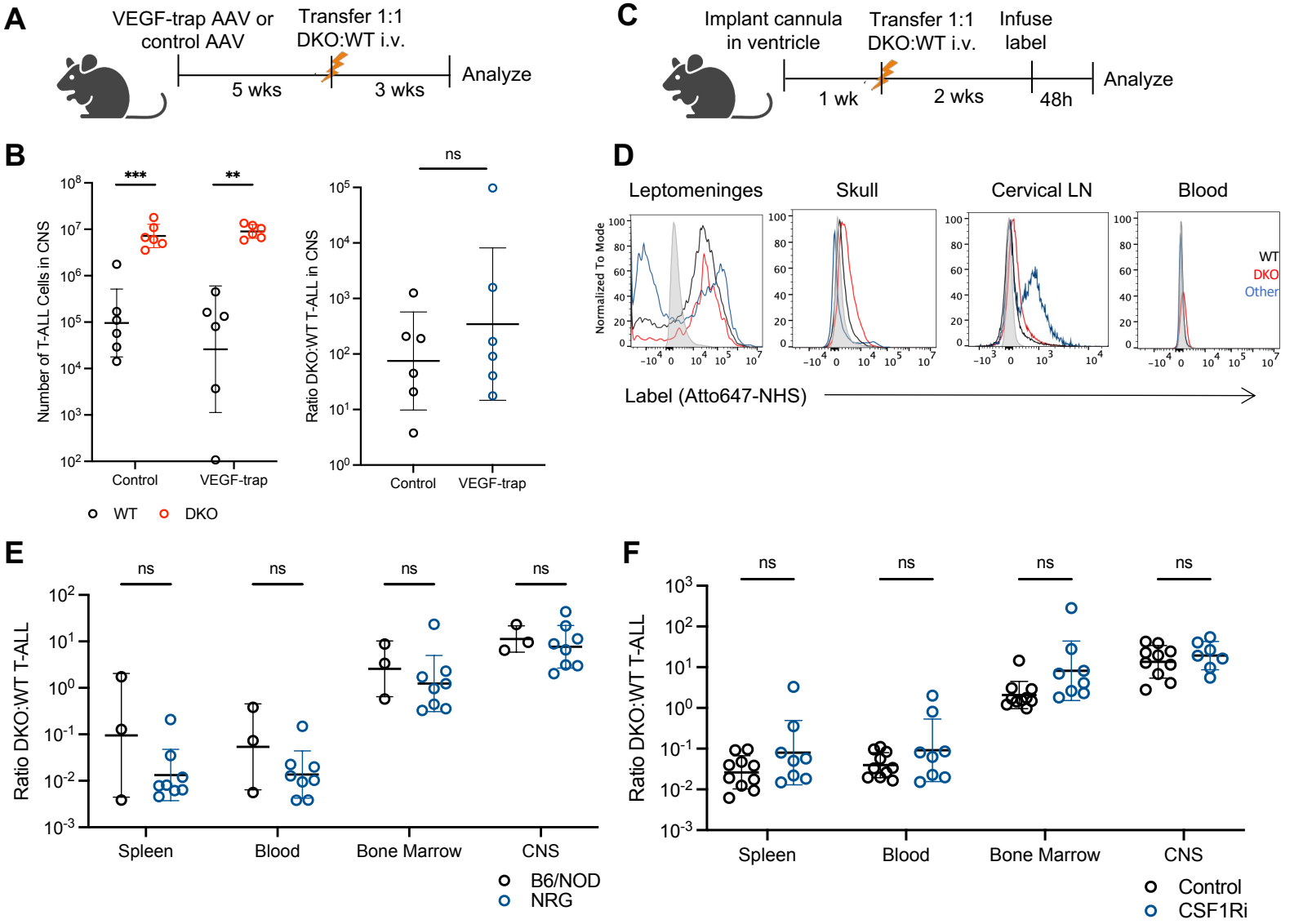

Fig. 3. Integrin-deficient T-ALL is unlikely to accumulate in the CNS due to enhanced exit or immune escape.
(A, B) WT mice were infected with AAV encoding a VEGF-trap or control AAV. 5 weeks later, mice were sub-lethally irradiated and injected i.v. with 1:1 DKO:WT T-ALL. At a humane endpoint, tissues were isolated, and T-ALL was enumerated. **(A)** Experiment design. **(B)** Number of WT (black) and DKO (red) T-ALL or ratio of DKO:WT T-ALL in the CNS of mice treated with either control AAV (n = 6) or AAV-VEGF-trap (n = 6). Data compiled from 2 experiments.
(C, D) WT mice were surgically implanted with an intra-cerebroventricular cannula. 1 week later, mice were sub-lethally irradiated and injected i.v. with 1:1 DKO:WT T-ALL. At mid-stage disease, a reactive label (Atto647-NHS-ester) was infused through the cannula into the left lateral ventricle. 48h later, tissues were isolated and labelled T-ALL cells were enumerated. **(C)** Experiment design. **(D)** Representative flow cytometry plots of Atto647 labelling in the indicated tissues. WT T-ALL, black; DKO T-ALL, red; other leukocytes, blue. Representative of 3 experiments, n = 6.
(E) NRG mice or WT controls (B6 or NOD) were sub-lethally irradiated, injected i.v. with 1:1 DKO:WT T-ALL, and analyzed at a humane endpoint. Ratio of DKO:WT T-ALL cells in controls (black; n = 3) or NRG mice (blue; n = 8). Data compiled from 2 experiments. **(F)** WT mice were fed either diet supplemented with a CSF1R inhibitor (PLX5622) or control diet for 1 week, sub-lethally irradiated and injected i.v. with 1:1 DKO:WT T-ALL, and maintained on either PLX5622 or control diet until a humane endpoint. Ratio of DKO:WT T-ALL in the indicated tissues of mice fed control diet (black; n = 10) or PLX5622 diet (blue; n = 8). Data compiled from 2 experiments.
Bars represent geometric mean and geometric SD. Statistics calculated on log-transformed data using unpaired t-test with Welch's correction. *$p \leq 0.05$, **$p \leq 0.01$, ***$p \leq 0.001$, ****$p \leq 0.0001$

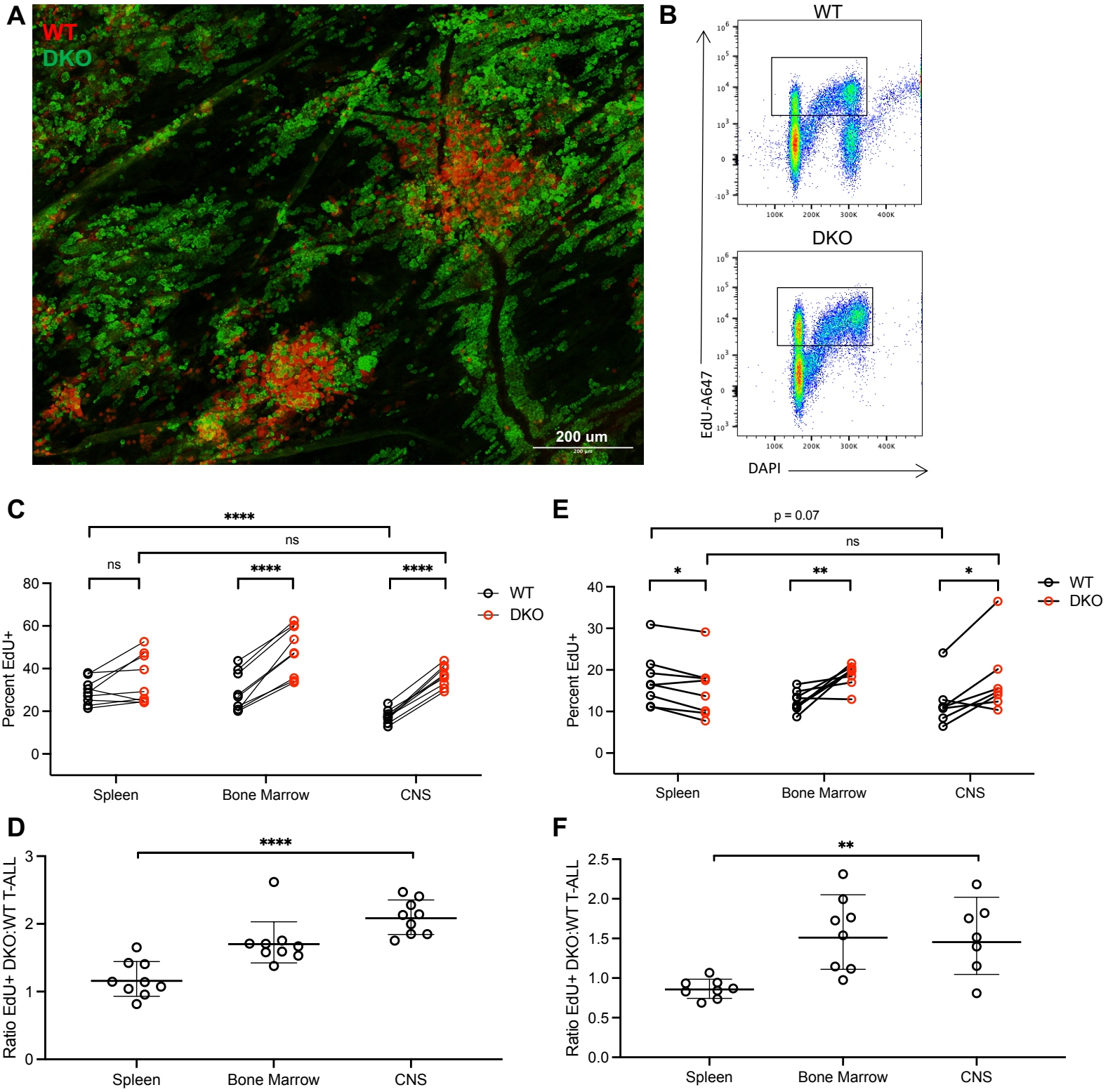

Fig. 4: Integrin-deficient T-ALL proliferates more than WT T-ALL in the CNS.
(A) Representative (of *n* = 12) immunofluorescence image of whole-mounted dural meninges of mice injected i.v. with 1:1 DKO:WT T-ALL. Mice were analyzed at mid-stage disease. Red, WT T-ALL; green, DKO T-ALL; scale bar, 200μm. **(B)** Representative flow cytometry gating to identify proliferating cells isolated from tissues of mice that received EdU 4 hours before analysis (in two intraperitoneal doses, 100 μg at -4h and 100 μg at -2h).
(C, D) Sub-lethally irradiated WT mice received 1:1 DKO:WT T-ALL cells i.v., and were analyzed at mid-stage disease. **(C)** The percent EdU+ of WT (black) or of DKO (red) T-ALL cells and **(D)** the ratio of % EdU+ DKO: % EdU+ WT T-ALL cells in the indicated tissues. Data compiled from 3 experiments; *n* = 9.
(E, F) As in (C, D) but for the CRISPR-WT and CRISPR-DKO pair of T-ALL lines. Data compiled from 4 experiments; *n* = 8.
For (C, E), statistics comparing WT and DKO within a tissue were calculated on logit-transformed data using paired t-test. Statistics comparing WT or DKO from CNS to spleen were calculated on logit-transformed data using unpaired t-test with Welch's correction. For (D, F), statistics calculated using unpaired t-test with Welch's correction, bars represent geometric mean and geometric SD. *p ≤ 0.05, **p ≤ 0.01, ***p ≤ 0.001, ****p ≤ 0.0001

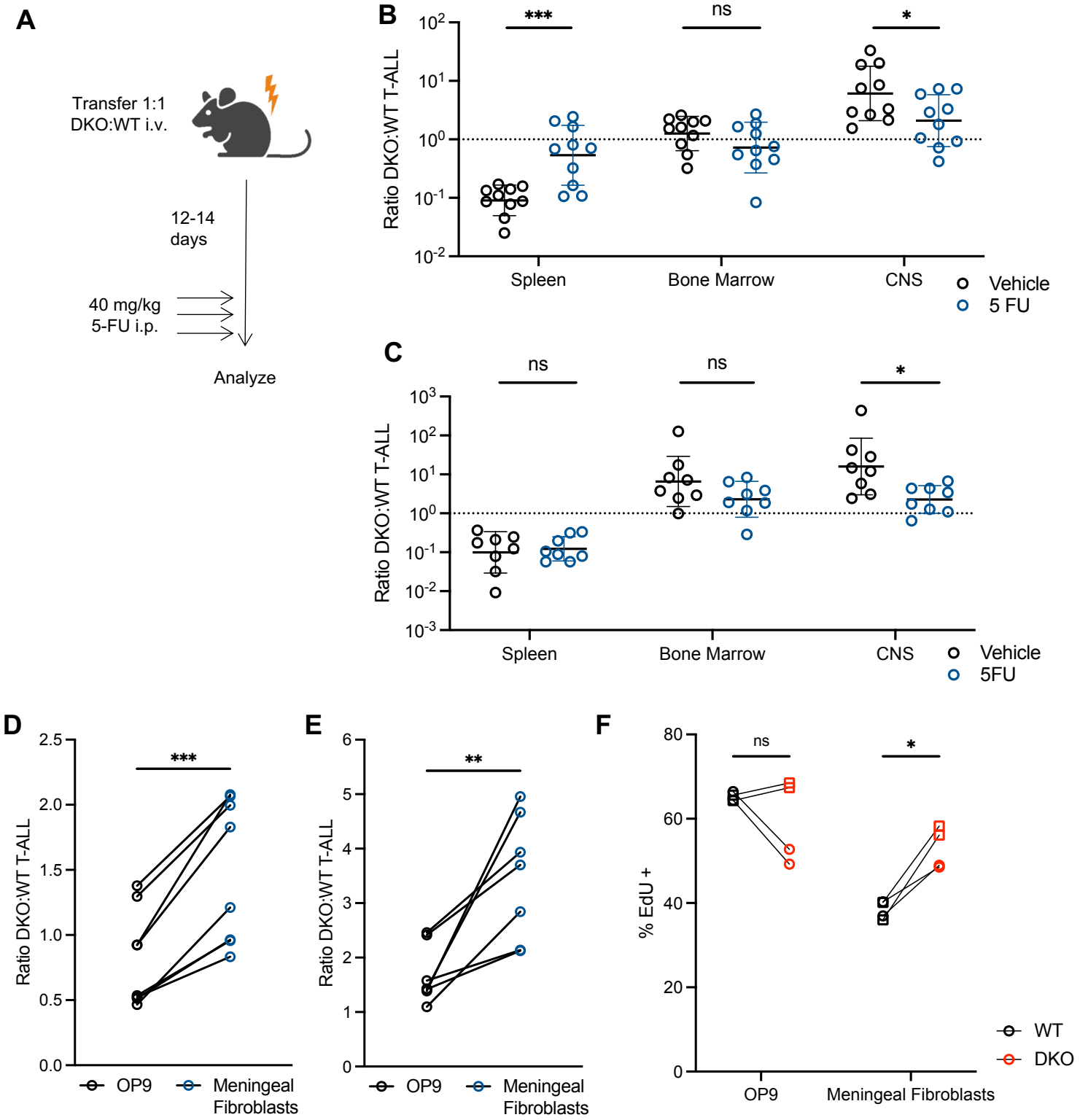

Fig. 5: Integrin-deficient T-ALL is more susceptible to chemotherapy targeting dividing cells.
(A) Sub-lethally irradiated WT mice received 1:1 DKO:WT T-ALL i.v., were treated daily i.p. with 40mg/kg 5-fluorouracil (5-FU) for 3 days at mid-stage disease (starting 12-14 days after T-ALL transfer), and were analyzed 24h after the last dose of 5-FU. **(B)** The ratio of DKO:WT T-ALL cells in vehicle-treated (black; *n* = 10) or 5FU-treated (blue; *n* = 10) mice. Data compiled from 2 experiments. **(C)** As in (B) but for the CRISPR-WT and CRISPR-DKO pair of T-ALL lines. Vehicle-treated (black; *n* = 8), 5FU-treated (blue; *n* = 8). Data compiled from 2 experiments.

(D-F) DKO and WT T-ALL cells (mixed at a 1:1 ratio) were cultured with fibroblasts isolated from the meninges of WT mice or with a comparison stromal cell line (OP9). **(D)** The ratio of DKO:WT T-ALL cells on meningeal fibroblasts (blue) or on OP9s (black) after three days. Data compiled from 4 experiments; *n* = 7. **(E)** As in (D) but with the CRISPR-WT and CRISPR-DKO cells. Data compiled from 4 experiments; *n* = 7. **(F)** The percent of EdU+ WT (black) or DKO (red) T-ALL cells after three days of culture on meningeal fibroblasts or OP9 cells. DKO and WT (circles) (*n* = 2) and CRISPR-DKO and CRISPR-WT (squares) (n = 2) both shown. Data collected from 2 experiments. For (D-F), each point represents the average of 2-3 technical replicates. Each meningeal fibroblast point represents an independent meningeal fibroblast preparation (isolated from a WT mouse) with paired OP9 replicate.
Bars represent geometric mean and geometric SD. Statistics calculated on log-transformed data using unpaired t-test with Welch's correction. *p ≤ 0.05, **p ≤ 0.01, ***p ≤ 0.001, ****p ≤ 0.0001.

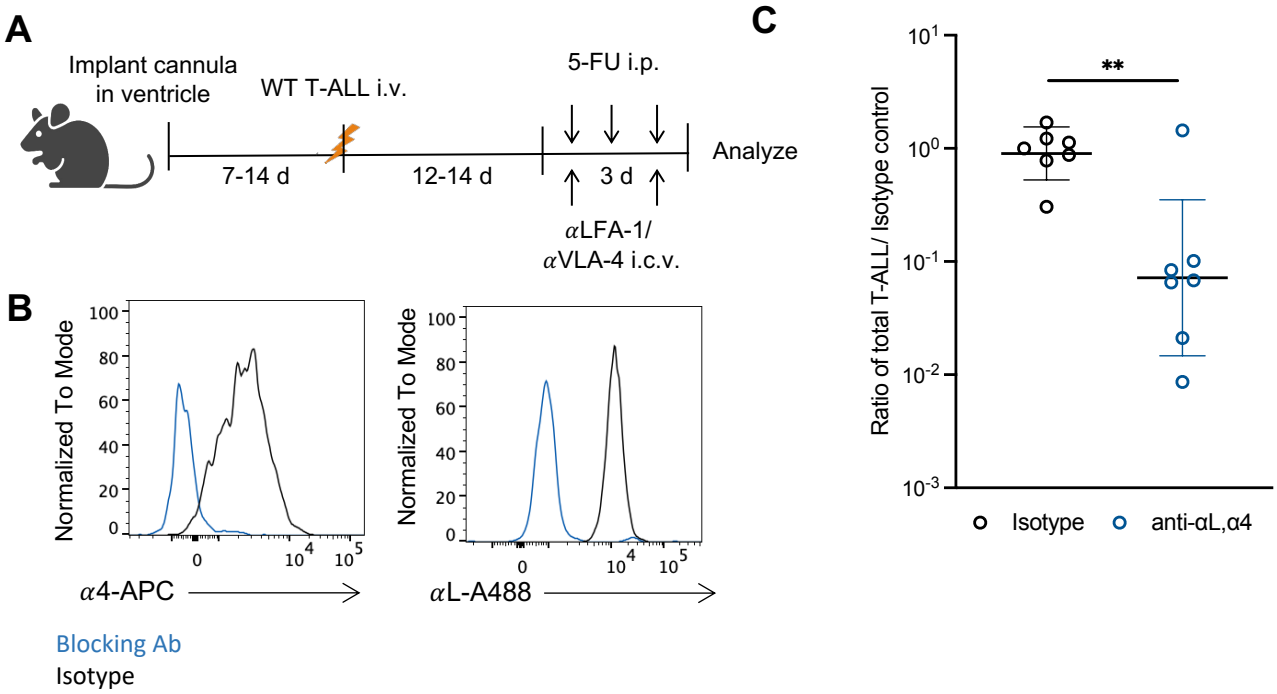

Fig. 6: Integrin blockade synergizes with chemotherapy targeting proliferating cells to limit CNS T-ALL.
(A) Mice were surgically implanted with a cannula in the left lateral ventricle. At least 7 days later, they were sub-lethally irradiated and injected i.v. with WT T-ALL. At mid-stage disease (12-14 days after T-ALL transfer), mice were injected i.p. with 40mg/kg 5-FU daily for three days. On days 1 and 3 of 5-FU treatment, mice received 5 microliter intraventricular infusions of isotype (47 microgram) or anti-LFA-1 and anti-VLA-4 (26 micrograms each) blocking antibodies. 24h after the last dose, tissues were isolated and T-ALL cells were enumerated. **(B)** Surface expression of α4 and αL integrins on WT T-ALL from the CNS after intra-cerebroventricular injection of LFA-1- and VLA-4- blocking antibodies (blue; representative of n = 7) or isotype (black; representative of n = 7). Representative of 4 experiments. **(D)** Total number of WT T-ALL in the CNS normalized to the average isotype control per experiment. Data compiled from 4 experiments; n = 7 pairs.
Bars represent geometric mean and geometric SD. Statistics calculated on log-transformed data using unpaired t-test with Welch's correction. *p ≤ 0.05, **p ≤ 0.01, ***p ≤ 0.001, ****p ≤ 0.0001